Lawrence Berkeley National Laboratory

Title
OXYGEN DIFFUSION IN HYPOSTOICHIOMETRIC URANIUM DIOXIDE

Permalink
https://escholarship.org/uc/item/35x7j0v4

Author
Kim, Kee Chul

Publication Date
1980-12-01

Peer reviewed

Lawrence Berkeley Laboratory
UNIVERSITY OF CALIFORNIA

Materials & Molecular Research Division

OXYGEN DIFFUSION IN HYPOSTOICHIOMETRIC URANIUM DIOXIDE

Kee Chul Kim
(Ph.D. thesis)

December 1980

OXYGEN DIFFUSION IN HYPOSTOICHIOMETRIC URANIUM DIOXIDE

Kee Chul Kim
Ph.D. Thesis

December 1980

Materials and Molecular Research Division
Department of Nuclear Engineering
Lawrence Berkeley Laboratory
University of California
Berkeley, CA 94720

iii

CONTENTS

ABSTRACT

OXYGEN DIFFUSION IN HYPOSTOICHIOMETRIC URANIUM DIOXIDE

Kee Chul Kim

Materials and Molecular Research Division
Department of Nuclear Engineering
Lawrence Berkeley Laboratory
University of California
Berkeley, California 94720

ABSTRACT

The tracer oxygen diffusivity in UO_{2-x} has been measured along
the lower two phase boundary. The diffusion couple consisted of two
matched hypostoichiometric uranium dioxide wafers, one enriched with
^{18}O and the other normal. These two were pressed together with a
bond of liquid uranium in between. After a diffusion anneal the ^{18}O
concentration profile was determined by ion microprobe mass analysis,
from which diffusion coefficients were obtained. The results showed
much higher diffusion coefficients than those of stoichiometric UO_2.
This directly proved that the major defect species in UO_{2-x} is the
anion vacancy. Activation energy of anion vacancy migration was
measured to be 11.7 ± 3.0 kcal/mole. A diffusion model established for
UO_2 and $UO_{2\pm x}$ showed that in stoichiometric UO_2 both interstitials
and vacancies contribute significantly to oxygen diffusion and neither
can be neglected; at $1400°C$ their contributions are about equal. This
model was extended to nearly stoichiometric $UO_{2\pm x}$ to predict oxygen
diffusion coefficients in these stoichiometry ranges. Also deduced
from the model were the Frenkel defect energy and entropy of 35.6 ± 9.2
kcal/mole and 13.2 ± 7.3 e.u., respectively. Using these values, the

contribution of Frenkel disorder to the excess enthalpy of UO_2 was evaluated. Calculation showed that Frenkel disorder accounts for 87 percent of the excess enthalpy at $3000°K$. A simple two band model for electronic excitation, with a band gap of 2.0 ev and effective electron mass of 7.6 m_e, accounted for the remainder of the excess enthalpy.

1. INTRODUCTION

1.1 Statement of the Topic

Transport phenomena in uranium dioxide are of importance in under-
standing the behavior of fuel elements during reactor operation. LMFBR
fuel pins are designed to be operated at higher temperatures and much
steeper temperature gradients than conventional thermal reactor fuels.
Across the 3 mm radius of a fuel pin, the temperature varies from about
2500°C at the center to about 700°C at the cladding. These extreme
conditions cause a variety of phenomena, including grain growth,
fission product migration, oxygen redistribution, and actinide
redistribution.

Oxygen diffusion is of special interest because of many different
contributions of the oxygen-uranium ratio and the oxygen potential to
the fundamental properties of the oxide. For example, the thermal
conductivity of the oxide changes with O/U ratio so that the local O/U
ratios affect the temperature profile within the fuel element. This
temperature profile is directly related to fuel restructuring, pore
migration, et c., and all these properties and phenomena are
interrelated.

The oxygen potential also plays an important role in many aspects
of the oxide fuel, from fuel fabrication to oxygen redistribution and
fuel-cladding reaction. The oxygen potential of the fuel determines
in large part whether or not the fuel can corrode the metallic cladding.
In order to minimize this reaction and accomodate the increase of the
oxygen potential by fission processes, the initial composition of the
oxide fuel for LMFBR is designed to be hypostoichiometric.

There have been many studies, both theoretical and experimental, of oxygen diffusion in stoichiometric UO_2 and hyperstoichiometric UO_{2+x} [1-11]. However, similar measurements in hypostoichiometric UO_{2-x} have never been attempted mainly because of UO_{2-x} is a defect structure stable only at high temperatures (see Fig. 1) so that its oxygen diffusion coefficient is most likely large enough to render conventional methods unworkable. For example, in the gas-solid isotopic exchange method, the gas phase mass transfer step or the surface isotopic exchange step may be rate-controlling. Also, since the equilibrium oxygen potential of hypostoichiometric uranium dioxide is extremely low, it would be very difficult, if not impossible, to control the gas stream to maintain stoichiometry during the diffusion anneal. Even if this could be achieved, it is doubtful that this small oxygen potential could be successfully isotopically monitored for diffusion measurements.

Together with thermodynamic information, transport data contribute greatly to the understanding of the defect structure of uranium oxide. Nevertheless, considerable uncertainty remains as to the fundamental aspects of the defect properties and transport mechanisms in the oxide. One of the difficulties lies in the fact that there are no transport data in UO_{2-x}, which is another reason why measurement of oxygen diffusion in UO_{2-x} is urgently needed.

Review of Previous Work

One of the earliest experiments reported was by Auskern et al. [2]. In this pioneering work, the oxygen self-diffusion coefficient in UO_2 was measured using the isotopic exchange reaction between
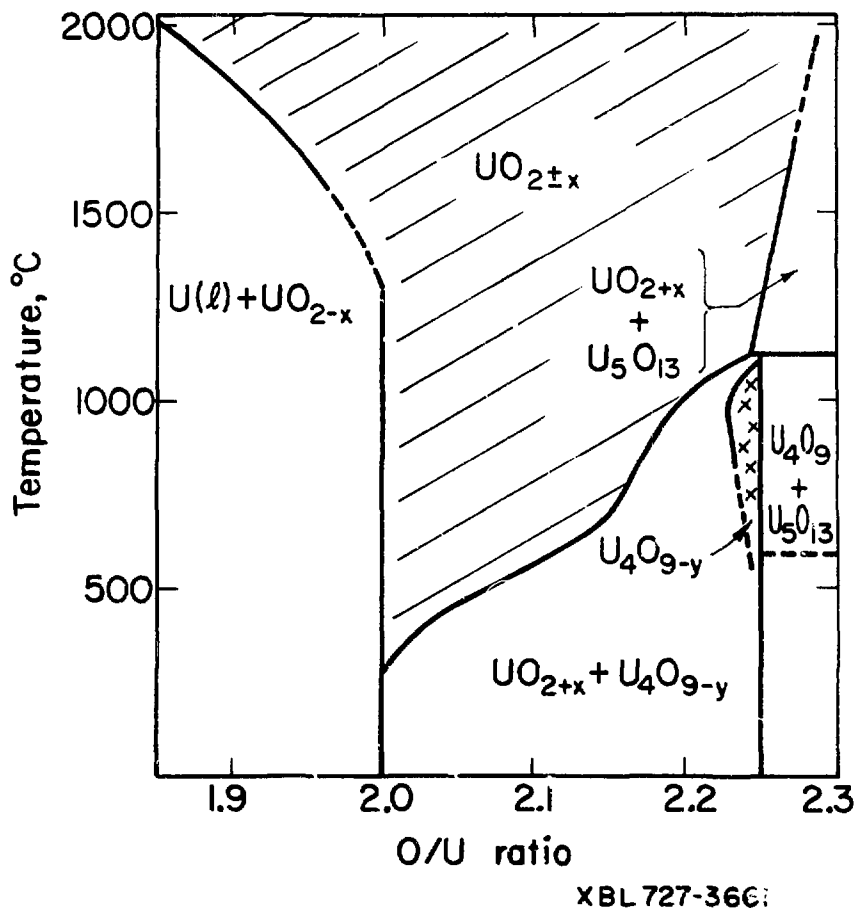
Figure 1. Oxygen-uranium phase-equilibrium system [18].

uranium dioxide powders and ^{18}O enriched carbon dioxide gas. They
reported that for essentially stoichiometric UO_2, the oxygen diffusion
coefficient in the temperature range 550-780°C could be represented by
$D = 1.2 \times 10^2 \exp(-65300/RT)$. The activation energy was verified in
later studies [1,7]. However, the pre-exponential factor was
abnormally high compared to later studies, both experimental [1] and
theoretical [9]. Systematic error due to the large variation in the
average particle diameter is a possible reason. Also reported was the
activation energy of 29.7 kcal/mole for hyperstoichiometric UO_{2+x}.
From these two activation energies Auskern et al. [2] calculated the
Frenkel defect formation energy of 70 kcal/mole, assuming that the
interstitialcy mechanism of oxygen diffusion applies to both UO_2 and
UO_{2+x}.

In an unpublished work, Roberts et al. [7] made a more systematic
attempt to obtain diffusion coefficients as a function of stoichiometry.
Using single crystal UO_2, they measured activation energies of
23 kcal/mole, 30 kcal/mole and 69 kcal/mole for stoichiometries of
2.03, 2.01, and 2.001, respectively in the temperature range of
1200-1600°C. These values are in fair agreement with those of Auskern
and Belle [2].

The two studies used the indirect gas-solid isotopic exchange
method, which possesses some inherent problems [1,4]. By performing a
direct diffusion couple experiment Marin et al. [1] attempted to over-
come the pitfalls of the gas exchange method. They employed massive
samples of normal UO_2 which were coated with a thin layer of UO_2 powder

highly enriched in ^{18}O. Then the couples were annealed, sectioned, and analyzed for ^{18}O penetration. The results were fitted by D=0.26exp(-59300/RT). The activation energy compares reasonably well with that found by Auskern et al. [2].

Using the same method, Contamin et al. [3] investigated the diffusion of oxygen in hyperstoichiometric UO_{2+x}. In the temperature range of 400-900°C an activation energy of 21 kcal/mole, independent of stoichiometry, was obtained. They systematically investigated the dependence of diffusion coefficient on stoichiometry as well as temperature, and they observed a sharp increase in diffusion coefficient with x of UO_{2+x} in the vicinity of x=0. An activation energy of 21 kcal/mole was obtained for $x \geq 0.006$. Also an attempt was made to correlate the D with x at various temperatures.

Similar work was reported by Murch et al. [6] for UO_{2+x}. For $UO_{2.08}$ they reported D=6.25 x 10^{-4} exp(-23100/RT) over the temperature range of 560-800°C. The pre-exponential factor and the activation energy were in good agreement with those of Contamin et al. [3].

Over the years it was thought that the anion vacancy migration energy might not be so high that the vacancy mechanism to be neglected as a contributor in stoichiometric and near-stoichiometric UO_2. This theory is supported largely by the experimental results on anion diffusion in other isostructural anion-deficient oxides such as CeO_{2-x} [12,13] and PuO_{2-x} [14,15]. In these studies the anion migration energy was measured in substantially hypostoichiometric specimen so that the diffusion process was controlled by the vacancy mechanism; also the activation energy would not contain the defect formation

energy. All of the results showed that the vacancy migration energies were within the range of 4-12 kcal/mole, which was compared with 21-30 kcal/mole for interstitial migration energy in UO_{2+x} mentioned earlier. In addition, Catlow et al. [16] substantiated these values with a theoretically determined value of 5.8 kcal/mole for vacancy migration in UO_{2-x}. From this standpoint, Murch et al. [9] attempted a theoretical calculation of diffusion coefficient of oxygen in $UO_{2\pm x}$, assuming that diffusion in UO_2 and $UO_{2\pm x}$ is controlled not only by interstitials but also by vacancies at the same time. Their predictions are reasonably close to the experimental values at high temperature stoichiometric UO_2 and to the data of Contamin et al. [3] for UO_{2+x}. Similar attempts were made by Breitung [8] using a simpler model.

2. THEORY

2.1 Methods of Diffusion Experiment

It was indicated in the previous chapter that conventional methods
are difficult to apply in hypostoichiometric UO_{2-x}. In this chapter
these methods will be reviewed and the theoretical basis of the present
experiment will be introduced.

2.1.1. Gas-Solid Isotopic Exchange Method

As applied in the works of Auskern et al. [2] and Roberts
et al. [7], the diffusion anneal is followed by a mass spectrometric
analysis of the $^{18}O/^{16}O$ ratio of the gas phase, one of the two
constituents (gas or solid) being tagged with ^{18}O. For this indirect
method to be workable in uranium dioxide, several experimental
conditions must be satified:

(1) Gas-solid surface exchange step should not be the rate con-
trolling step.

(2) Gas phase mass transfer could not be the rate controlling
step.

(3) The partial pressure of oxygen in the gas should be matched to
the equilibrium oxygen potential of the solid urania in order
to maintain the original stoichiometry throughout the experi-
ment

Employing this method in hypostoichiometric UO_{2-x} might violate
the first and second conditions because the UO_{2-x} phase exists only
at high temperatures and therefore the diffusion in solid phase is
probably extremely fast. In regard to the third condition, since the
oxide should be in the form of powder in order to provide large surface

area, the stoichiometry of the samples would be extremely vulnerable to the surrounding gas, especially at the high temperatures.

The most convenient way of achieving a desired oxygen potentials is by a mixture of CO_2-CO or H_2O-H_2. For example, the equilibrium oxygen potential of $UO_{1.98}$ at $1700°C$ is -170 kcal/mole, which is equivalent to $CO_2/CO_0 = 4 \times 10^{-13}$ and $H_2O/H_2 = 10^{-6}$ at this temperature. The CO_2/CO ratio is so low that it would be extremely difficult to achieve. The H_2O/H_2 ratio could be controlled in this range fairly well, but not easily. However, since the H_2O is the only oxygen-carrying species, it would be difficult to detect minute changes in the ^{18}O fraction in such a small amount.

From these standpoints, this method does not seem to be appropriate for UO_{2-x}.

2.1.2 Diffusion Couple (layer-solid) Method

In this method two UO_2 pellets, one enriched with ^{18}O and the other normal, are placed in contact. ^{18}O and ^{16}O interdiffuse when the couple is heated. Unlike the gas-solid isotopic exchange method, this is a direct surement of diffusion and there are none of the inherent systematic errors or difficulties in using gases. However, accomplishing a truly good contact between two solids is difficult. Contamin et al. [2] overcame this difficulty by depositing a thin layer of $U^{18}O_2$ (10-20 um) by decanting a suspension of $U^{18}O_2$ in ethyl alcohol. Pairs of samples with enriched layers in contact were annealed in vacuum for several hours under pressure at low temperature

in order to promote good contact. They were then diffusion annealed in hydrogen and argon, and then sectioned to determine ^{18}O profile using spark mass spectrometry and ion mass analysis.

Murch et al. [6] used a technique that differed only in that a thicker deposit (~150 μm) of ^{18}O-enriched UO_{2+x} was used.

There are numerous ways to investigate the concentration profile other than by spark mass spectrometry and ion mass analysis, which are described elsewhere [11].

2.2 Experimental Technique of the Present Study (Solid-Solid Method)

In order to eliminate the experimental difficulties and uncertainties of a layer-bulk diffusion couple, a bulk-bulk couple was utilized instead. The diffusion couple consisted of two UO_{2-x} wafers, one of which was enriched with ^{18}O. As mentioned previously, this technique has the difficulty in achieving good contact between two wafers. Calculation showed that the vapor pressure of UO_2 is too low for sufficient oxygen transport from one side to another through a vacuum gap.

To avoid this interfacial resistance, the wafers were bonded together by liquid uranium. Liquid uranium is believed to have a sufficiently high solubility [17-20] so that the liquid metal bond should transport oxygen from one wafer to the other quite efficiently. This technique is equivalent to reduction of the heat transfer resistance in the fuel-cladding gap of carbide fuel pins by sodium bonding.

However, since the diffusion coefficient in liquid uranium is different from that in solid urania, the problem had to be analyzed with this effect included.

In order not to perturb the stoichiometry of the wafers by the presence of liquid uranium, the experiments were performed only in $U(\cdot)+UO_{2-x}$ two-phase region. In this system, the stoichiometries to be studied were fixed automatically by the temperatures and therefore the diffusion measurements would be only on O/U ratios along the lower phase boundary (Fig. 1).

2.3 Theoretical Analysis

In order to measure the diffusion coefficient, the ^{18}O profile has to be fitted to an analytic solution of the diffusion equation, which should include the effect of the liquid uranium layer at the interface. This can be obtained by solving the diffusion equation with appropriate boundary conditions. The diffusion equation can be written in dimensionless form:

$$\frac{\partial \phi}{\partial \tau} = \frac{\partial^2 \phi}{\partial \eta^2} \tag{1}$$

where $\phi = \dfrac{y-y_0}{y_1-y_0}$, $y = {}^{18}O$ isotopic ratio $= \dfrac{^{18}O}{^{18}O+^{16}O}$

y_i = initial isotopic ratio of ^{18}O in ^{18}O-enriched wafer

y_0 = initial isotopic ratio of ^{18}O in normal wafer.

$\tau = Dt/\ell^2$, D is diffusion coefficient, t is time, ℓ is the thickness of one wafer, $\eta = \dfrac{z}{\ell}$, z is the distance measured from the surface of the enriched wafer.

The geometry of the diffusion couple is depicted in Fig. 2. The initial condition can be written as:

$$\text{I.C.} \quad \phi(\eta, 0) = 1 \quad , \quad 0 < \eta < 1$$

$$\phi(\eta, 0) = 0 \quad , \quad 1 < \eta < 2 \tag{2}$$

Since both ends are insulated;

$$\text{B.C.1} \quad \frac{\partial \phi}{\partial \eta} = 0 \text{ at } \eta = 0$$

$$\frac{\partial \phi}{\partial \eta} = 0 \text{ at } \eta = 2 \tag{3}$$

Throughout the calculation it is assumed that the liquid uranium thickness δ is very small, i.e., $\delta \ll \ell$ and that the wafers are infinite slabs.

At the interface, the ^{18}O flux is continuous:

$$J = -D \left[\frac{\partial C_{18}}{\partial z} \right]_{z^-} = -D \left[\frac{\partial C_{18}}{\partial z} \right]_{z^+} \tag{4}$$

where C_{18} is the concentration of ^{18}O in UO_{2-x}.

$$C_{18} = C_0 y = C_0 [y_0 + (y_1 - y_0)\phi] \tag{5}$$

where C_0 is the total oxygen concentration in UO_{2-x}.
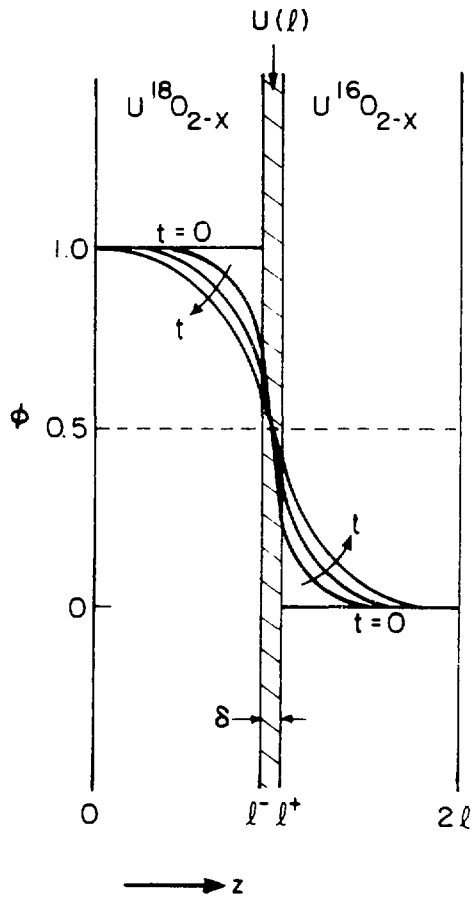
Figure 2. Geometry of the diffusion couple
bonded by liquid uranium.

Thus,

$$J = -\frac{DC_0(y_1-y_0)}{2}\left[\frac{\partial\phi}{\partial n}\right]_{1^-} = \frac{DC_0(y_1-y_0)}{2}\left[\frac{\partial\phi}{\partial n}\right]_{1^+} \tag{6}$$

The ^{18}O flux in the liquid uranium can be written as:

$$J = D_0^u \frac{c_{13}^u|_{1^-} - c_{13}^u|_{1^+}}{s} \tag{7}$$

D_0^u is oxygen diffusion coefficient in liquid uranium, c_{13}^u is the ^{18}O concentration in the liquid uranium, and s is the thickness of the liquid uranium. Assuming isotopic equilibrium at the interface of UO_{2-x} and liquid uranium,

$$c_{13}^u = c_0^u y = c_0^u[y_0+(y_1-y_0)\phi] \tag{8}$$

where C_0^u is the solubility of oxygen in liquid uranium. Thus, from Eq. (7)

$$J = \frac{D_0^u c_0^u}{s}(y_1-y_0)(\phi_{1^-} - \phi_{1^+}) \tag{9}$$

From the symmetric nature of the problem, at the center of the liquid uranium layer, $\phi = 1/2$ at all times, and Eq. (9) can be replaced by:

$$J = \frac{D_o^J C_o^u}{(\delta/2)} (y_1 - y_0)(\phi_{1^-} - \frac{1}{2}) = \frac{D_o^u C_o^u}{(\delta/2)} (y_1 - y_0)(\frac{1}{2} - \phi_{1^+}) \tag{10}$$

Thus, from Eqs. (6) and (10), we have:

$$B.C.2 \qquad -\frac{\partial \phi}{\partial n}\Big\}_{1^-} = -B(\phi_{1^-} - \frac{1}{2})$$

$$-\frac{\partial \phi}{\partial n}\Big\}_{1^+} = -B (\frac{1}{2} - \phi_{1^+}) \tag{11}$$

where $B = \frac{D_o^u}{D} \frac{r}{(\delta/2)} \frac{y_o^u}{C_o}$. $\tag{12}$

The parameter B represents the overall conductance of the liquid
uranium layer for oxygen. The higher the value B, the less resistance
is offered by the liquid uranium layer to oxygen transport across the
interface. This parameter depends mainly upon the solubility of oxygen
in liquid uranium, which is not very well established experimentally
and shows a large disagreement among different investigators [17-20].
However, even use of the most pessimistic data yields B values that
permit modest diffusion rates. The only factor in B that can be con-
trolled is s. Therefore, it is important to minimize the thickness of
the liquid uranium layer.

From Eqs. (1), (2), (3), and (12), ϕ can be solved to yield [21]:

$$\phi = \frac{1}{2} + \sum_{n=1}^{\cdot} e^{-Da_n^2 t} \frac{\{(a_n)^2 + B^2\} \cos(a_n z)}{\{(a_n)^2 + B^2 + B\}} \frac{\sin(a_n)}{a_n} \tag{13}$$

x_n's are positive roots of $(\alpha\ell)\tan(\alpha\ell)-B=0$. The best values of D and B are sought to fit the data points from the diffusion experiments to Eq. (13).

.

3. EXPERIMENTAL - SAMPLE PREPARATION

As was indicated previously, two reduced UO_{2-x} wafers are needed: one enriched in ^{18}O and the other normal. The overall procedure for sample preparation can be described as follows:

(1) Preparation of $U^{18}O_2$

(2) Reduction of UO_2 and $U^{18}O_2$

(3) Determination of stoichiometry of the reduced sample.

Each step is described in detail below.

Preparation of $U^{18}O_2$

i Theory

^{16}O atoms in UO_2 were replaced by ^{18}O using ^{18}O-enriched water (95.1 percent ^{18}O-enriched water was obtained from Mound Laboratory), at high temperature:

$$U^{16}O_2 + H_2^{18}O \rightarrow U^{18}O_2 + H_2^{16}O \tag{14}$$

In doing so, it was necessary to maintain the original stoichiometry, This was achieved by mixing H_2 and $H_2^{18}O$ in the ratio that yield the equilibrium oxygen potential of stoichiometric UO_2. This can be formulated in the following way:

$$H_2 + \tfrac{1}{2} O_2 \rightleftharpoons H_2O \tag{15}$$

$$K = \frac{p_{H_2O}}{p_{H_2}(p_{O_2})^{1/2}} = \exp(-\Delta G^0/RT) \ . \tag{16}$$

P's are partial pressures and ΔG^O is standard free energy of reaction (16).

Thus,

$$P_{O_2}^{1/2} = \frac{P_{H_2O}}{P_{H_2}} \exp(\Delta G^O/RT) \tag{17}$$

The oxygen potential is defined as:

$$\overline{\Delta G}_{O_2} = RT \ln P_{O_2} \tag{18}$$

From Eqs. (17) and (18),

$$\overline{\Delta G}_{O_2} = 2RT \ln \frac{P_{H_2O}}{P_{H_2}} + 2\Delta G^O \tag{19}$$

ΔG^O , in cal/mole, is very well known [22]:

$$\Delta G^O = -57250 - 0.21 \ T + 1.948 \ T\ln T \tag{20}$$

Since the oxygen potential of UO_2 is also well known [23-29], the ratio H_2O/H_2 can be determined from Eq. (19).

Oxygen potential of $UO_{2\pm x}$ is shown graphically in Fig. 3. As can be seen, the oxygen potential changes very sharply in the vicinity of stoichiometric UO_2, e.g., from -140 to -70 kcal/mole at 1800°C. Due to this effect, virtually any oxygen potential within this range would be satisfactory for maintaining stoichiometric UO_2. Due to this effect, virtually any oxygen potential within this range would be satisfactory for maintaining stoichiometric UO_2.
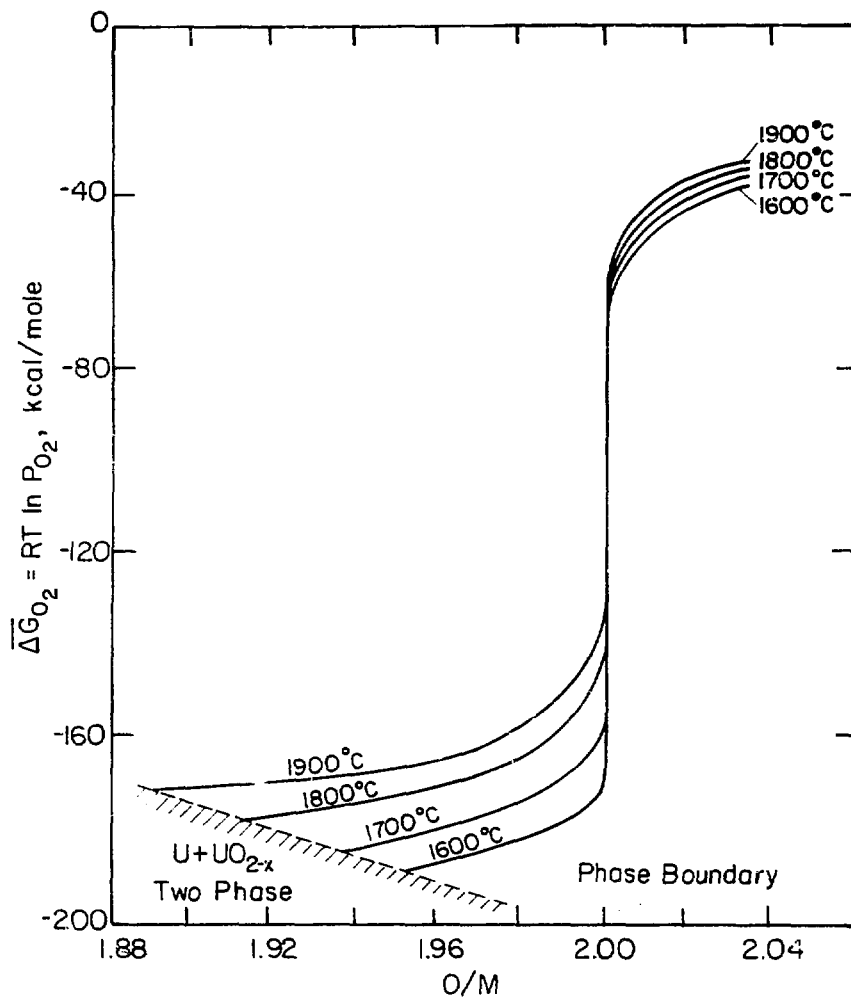
XBL792-5670

Figure 3. Variation of oxygen potential with temperature and O/U
           ratio [54]. The two-phase boundary is based on Ref. [38].

To promote a fast reaction, high temperature and high ratio of $H_2^{18}O/H_2$ were preferred, yet the temperature had to be low enough to prevent a significant evaporation. To satisfy these requirements, the conditions of $H_2^{18}O/H_2 = 10^{-2}$ and $T = 1500°C$ were chosen, which would yield $\overline{\Delta G}_{O_2} = -103$ kcal/mole.

The desired $H_2^{18}O/H_2$ ratio could be obtained by saturating H_2 with $H_2^{18}O$. The saturation was achieved by flowing H_2 gas at 1 atm through $H_2^{18}O$ the temperature of which was controlled so that it would yield the predetermined $H_2^{18}O/H_2$ ratio. Although the H_2 flowed through the $H_2^{18}O$ in the form of tiny bubbles, the exit gas might have been slightly undersaturated. However, due to the wide range of equilibrium oxygen potential of stoichiometric UO_2, this slight uncertainty was acceptable.

3.1.2 Apparatus

Figure 4 depicts the overall system which was used for all aspects of sample preparation.

The gas lines were made from 1/4 in. O.D. stainless steel tube. To minimize contamination, high purity gas valves were used exclusively and only stainless steel Swagelok-type fittings were used for connections. The use of O-ring type fittings and valves was avoided. This design was particularly important for the UO_2 reduction step, because even a trace of H_2O in H_2 would inhibit or limit the capability of reduction (see Fig. 3).
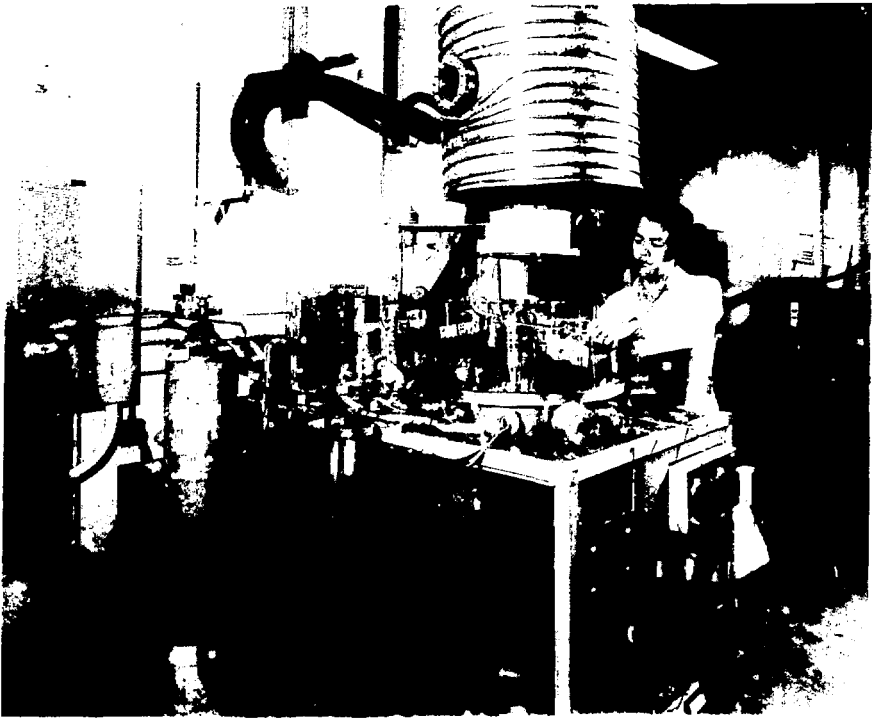
To prevent a back-diffusion of air into the system the gas was vented through diffusion pump oil which separated the system from the atmosphere.
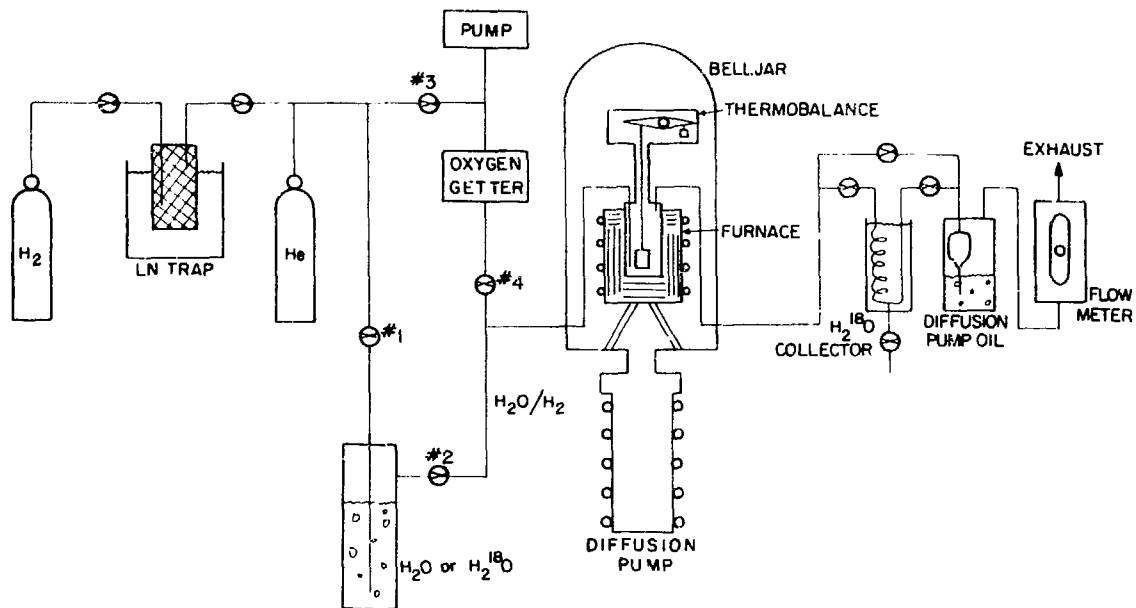
Figure 4.   Line diagram of the system.

XBL 8010-6097

YDP 800 13020

Figure 5. Photograph of overall apparatus.

3.1.2.1 Furnace

Shown in Fig. 6 is a detailed view of the furnace. The UO_2 specimen was placed inside a molybdenum crucible, which was 1 in. O.D. and 6 in. long, and electron beam welded to a 3.5 in. wide molybdenum flange.

A tungsten mesh element, 3 in. diameter and 6 in. long, was used to heat the furace. The temperature was controlled by the voltage applied to the heating element which was surrounded by a series of tungsten radiation shields to minimize the heat loss and to protect the outer shell of the furance, which was cooled by water.

The gas was fed into the bottom of the crucible by a 1/8 in. molybdenum tube and flowed upward from then on. A rhenium rig was designed to hold several UO_2 wafers in an upright position.

The entire furnace was contained in a belljar which was under a vacuum for operation. A pressure of 10^{-6} torr could be obtained using a 6 in. diffusion pump. During furnace operation $5-9 \times 10^{-6}$ torr could be maintained.

The temperature was measured by W3%Re-W25%Re thermocouple which was adjacent to the specimen inside the molybdenum crucible.

3.1.2.2 $H_2^{18}O - H_2$ Controlling System

The H_2 was saturated with $H_2^{18}O$ in a Pyrex tube where tiny bubbles were generated in a $H_2^{18}O$ by flowing H_2 through a porous glass frit (see Fig. 7). The tube was immersed in a water bath which was temperature controlled by Neslab PBC-2 bath cooler within $\pm 0.5°C$.

23
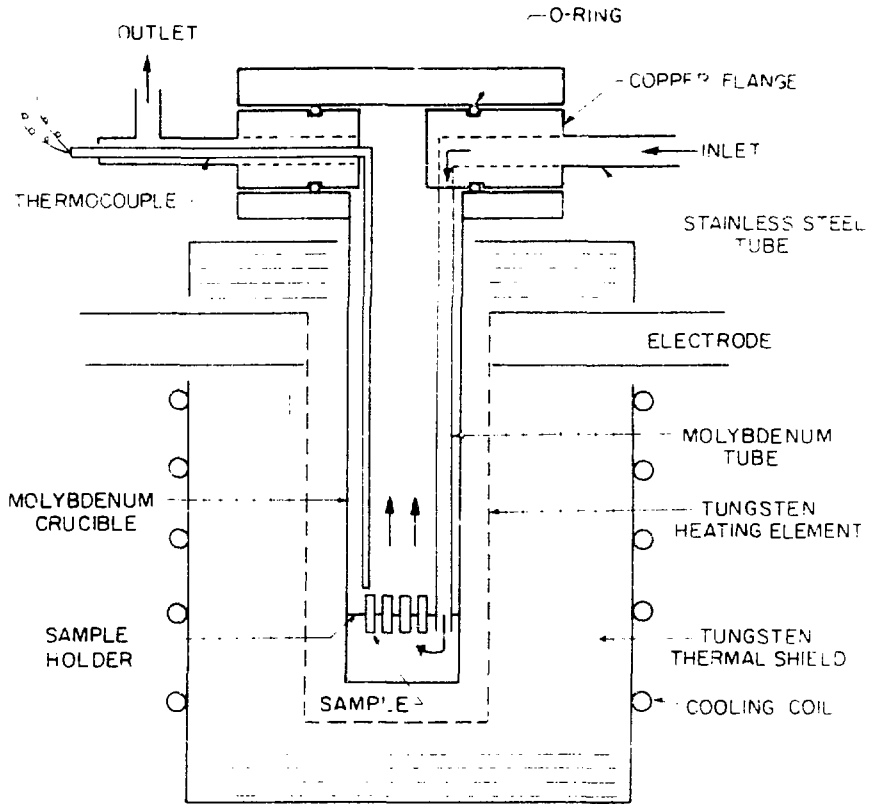
XBL 8010-6098

Figure 6.   Detailed view of the furnace.
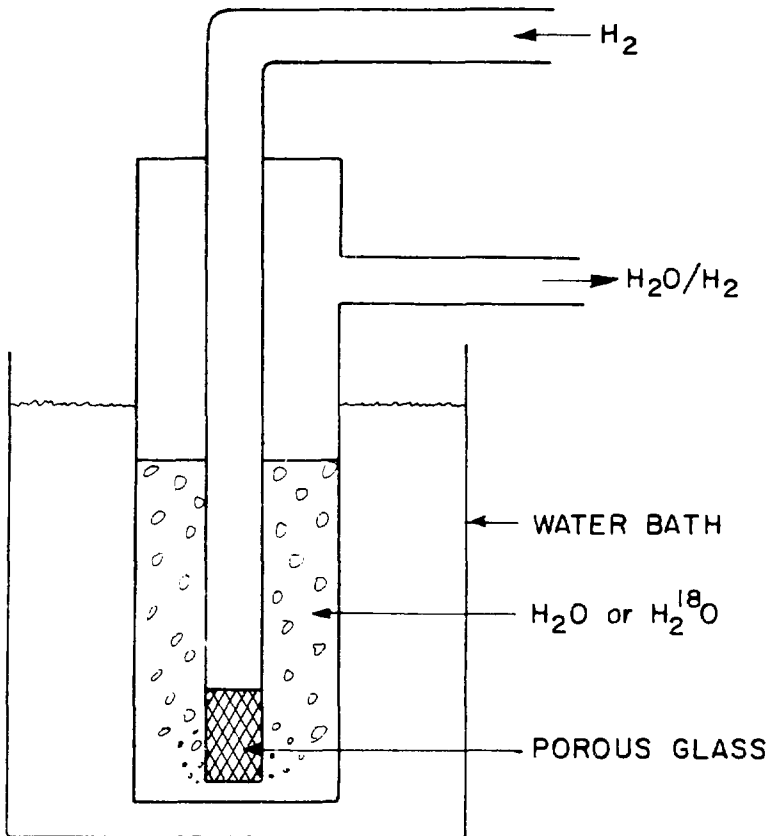
XBL 8010-6099

Figure 7. H_2O - H_2 controller.

Since only a small portion of $H_2^{18}O$ in the mixture reacted with
UO_2, it was necessary to collect and recycle this valuable water from
the outlet. First, the outlet from the furnace went through a cold
trap the temperature of which was maintained slightly above $0°C$. The
temperature was chosen to prevent blocking the tube by ice formation.
After this, the gas went through a liquid nitrogen cooled trap which
collected the remaining $H_2^{18}O$. Of course this recycled water was
slightly less enriched than the original $H_2^{18}O$.

3.1.3 UO_2 Wafer Preparation

UO_2 pellets of 1.17 cm diameter, 1.5 cm high were provided by the
General Electric Co., Vallecitos.

Wafers of approximately 1.4-1.1 mm thickness were cut from the
pellets and polished using silicon carbide abrasives and diamond paste.
Polishing promoted a good contact in the diffusion couple. It was
equally important that the thickness of a wafer should be uniform.
Otherwise the contact of the two wafers would not be parallel.
Thicknesses of the two wafers were matched within 0.02 mm for each
set, one of which was later enriched with ^{18}O.

Single crystal UO_2 pellets of 1 in. diameter were obtained from
the Georgia Institute of Technology. A single crystal portion, about
1.2 cm in the center, was cut out after slicing them into 1.1 mm thick
wafers. The same procedure employed for polycrystalline specimens was
used for grinding and polishing.

Table 1. Impurities in UO_2 pellets

Element	PPM	Element	PPM	Element	PPM
Mg	<1	Cu	<0.4	Sn	<1
Si	10	Fe	13	V	<5
Cd	<0.3	Pb	<0.3	Zn	<1.5
B	0.4	Mn	<0.3	Sb	<0.5
Al	<5	Mo	<5	Be	<0.5
Ca	1	Ni	<2	Bi	<0.2
Cr	<2	Ag	<0.1	P	<3.7
Co	<2.7	Na	<8	Ti	<0.3

3.1.4 Procedure for Enrichment of UO_2 in Oxygen-18

(1) Measure the weight of the sample: Before placing in the
furnace, the weight was measured using a Mettler microbalance
to compare with the weight after the exchange reaction.

(2) Pump out the entire system: Before each run the entire
system was pumped out while heating up the samples to 300°C
in order to degas them.

(3) Cool down to room temperature and fill the system with helium.

(4) Start flowing helium at a rate of 10 cc/sec; with valves
No. 1 and No. 2 in Fig. 4 closed and valves No. 3 and No. 4
open.

(5) Turn on the furnace and heat up to 800°C; To prevent the
samples from cracking by the thermal stress, the furnace was
heated up slowly.

(6) Shut off helium flow.

(7) Start flowing hydrogen.

(3) Set tne hydrogen flow rate at 5 cc/sec.

(9) Heat up to $1500°C$.

(10) Flow $H_2^{13}O-H_2$ for 38-48 nours; with valves No. 1 and
No. 2 open and No. 3 and No. 4 closed. The temperature of
$H_2^{13}O$ was maintained at $7.5°C$ wnicn would yield
$H_2^{13}O/H_2 = 10^{-2}$

(11) Stop flowing $H_2^{13}O/H_2$ and anneal for 5 nours; Samples
were annealed in order to acnieve a uniform ^{13}O concentra-
tion in UO_2. Since they were to be reduced at nigner
temperature ($\sim 2000°C$), where the diffusion would be very
fast, even if there nad been a slight nonuniformity at tnis
stage it was considered to be immaterial.

(12) Cool down to $800°C$.

(13) Start flowing nelium.

(14) Cool down to room temperature.

(15) Take out the sample and measure tne final weignt.

Exactly the same procedure, except for using normal water instead of
$H_2^{13}O$, was applied to the counterpart of the matched samole in order
to impose an identical nistory. Since suostantial grain growtn was
ooserved after 48 nours of reaction, tnis process was considered to be
an essential step, especially for the polycrystalline samples. As was
expected, no significant weignt cnanges were ooserved wnen normal water
was used. Therefore, tne following conclusions were drawn:

(1) There had been no stoichiometry change due to this
    procedure.

(2) There had been no significant vaporization.

(3) All the weight change observed when using $H_2^{18}O-H_2$
    should be attributed to the substitution of ^{16}O by ^{18}O.

4.1.6 Results of the Isotopic Enrichment Process

The degree of enrichment can be calculated from the weight change
and the fractional weight increase for 100 percent substitution of
^{16}O by ^{18}O for 1 gram UO_2 sample (0.0141):

$$\text{enrichment} = \frac{(W_f - W_i)/W_i}{0.0141} \quad , \tag{21}$$

where W_i = initial weight

W_f = final weight.

Shown in the following Table 2 are results of two different
batches. The thinner the wafer, the higher the enrichment, which
indicates that the diffusion of oxygen UO_2 was one of the rate con-
trolling steps. This result means that there had been a nonuniformity
in ^{18}O concentration in the sample. However, at 1500°C the oxygen
diffusion coefficient in UO_2 is approximately 5×10^{-8} cm^2/sec [1]
and with this diffusion coefficient, 5 hours of annealing should have
relieved most of the nonuniformity and the subsequent 4 hours reduction
at high temperature (2000°C) would virtually eliminate the non-
uniformity. This expectation was proved later when the diffusion
couple was analyzed after the diffusion experiment, and showed a flat

^{13}O profile near the edge where the diffusion had not yet

penetrated. This will be discussed in detail later.

Table 2. Typical weight changes after oxygen exchange reaction, and
the calculated enrichment.

Batch No. 1

Thickness, mm	w_i, gm	w_F, gm	enrichment, %
0.465	...2147.	1.120030	73.5
0.940	1.112645	1.134875	71.3
0.914	...943540	1.104923	71.5
0.839	1.163300	1.0301.5	75.1
0.864	.443.19	1..146?	77.7
0.938	0.444145	0.45553..	50.3
0.972	.39..45	745	41.1

Batch No. 2

Thickness, mm	w_i, gm	w_F, gm	enrichment, %
1.244	..154345	...11963.	44.5
1.27.	1.422312	1.433321	45.1
...158	1.364920	1.371425.	15.1
1.156	..361141	1.371571	47.3

4.1 High Temperature Gas Phase Mass Transfer Study of UO₂

The oxygen deficient, hypostoichiometric, UO_{2-x} can be prepared
by hydrogen reduction of UO₂ at high temperature:

$$UO_2 + xH_2 \rightarrow UO_{2-x} + xH_2O \qquad (22)$$

The course of the reduction process was followed by a thermobalance. At high temperatures, however, the sample loses weight not only by reduction but by vaporization. Therefore, in order to study the reduction/evaporation process and to understand the capability of the system, it was necessary to conduct a systematic mass transfer study.

3.2.1 Apparatus

3.2.1.1 Thermobalance

The furnace was basically the same as the one used in the oxygen exchange reaction except that it was equipped with a Cann RG Electrobalance. The balance consisted of a control unit and a weighing assembly. A Heath dual pen chart recorder adopted for 1 mv signal was used for the readout of the balance. It had a capacity of 2.5 gm, readability of 0.5 percent of 1 mv recorder (equivalent to ultimate readability of 0.1 ug).

The weighing unit was housed in a leak-tight aluminum chamber which was maintained at a constant temperature by cooling water. An aluminum hangdown tube which was connected to a 3-1/2 in. flange was used to suspend the sample below the balance into the furnace (see Figs. 9 and 10).

In order to minimize the radiation from the furnace into the balance chamber, the hangdown tube needed to be narrow and long. Yet, at the same time the tube should be wide enough to keep the suspension wire from rubbing against the wall which would cause enormous noise in the readout. A 0.4 in. I.D., 1/2 in. O.D., 5 in. long aluminum tube was used. It was essential to have an absolutely straight wire to prevent rubbing against the tube wall, yet very light in weight. Therefore,
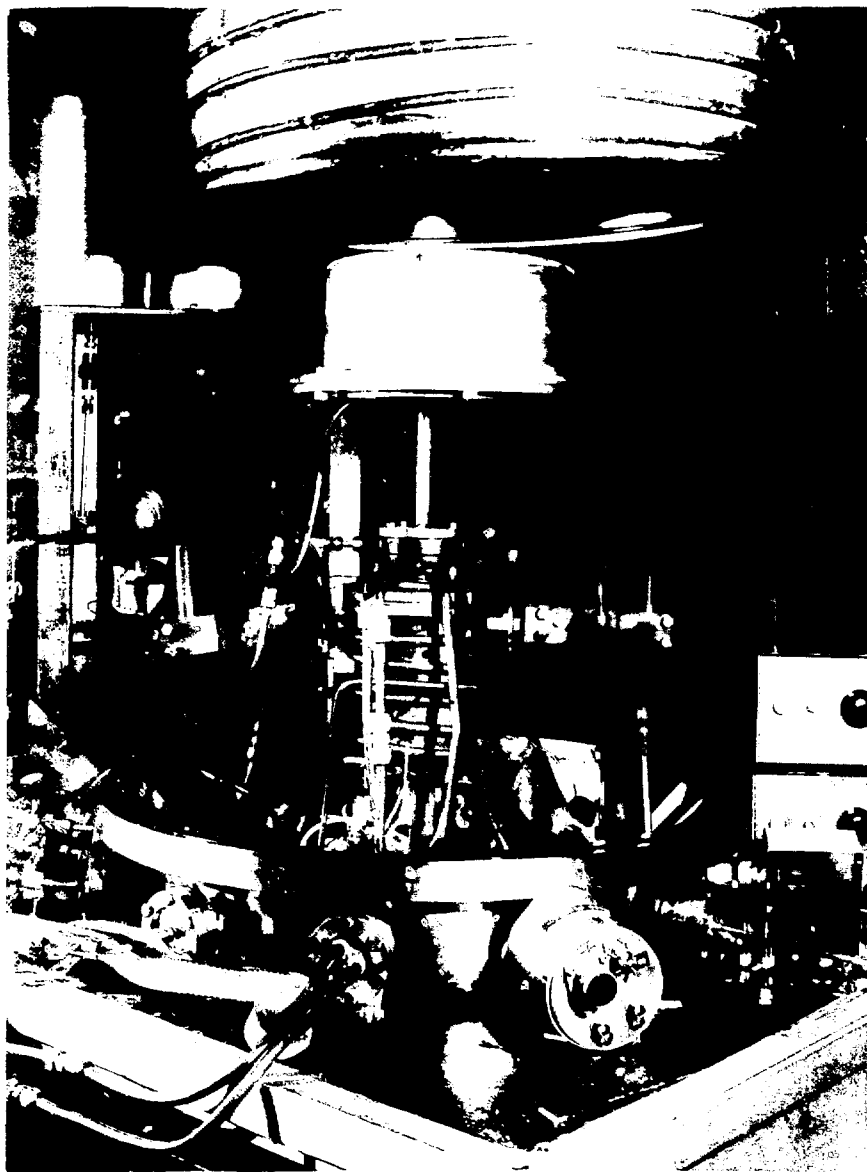
X56 0° 1.2's

Figure ... wiring unit of damp 71 lasted lasos.
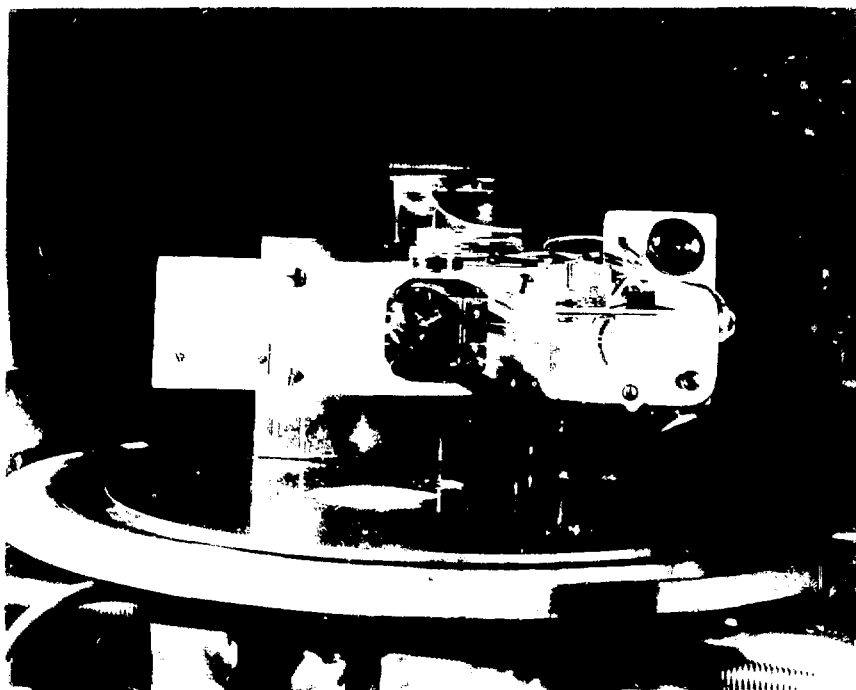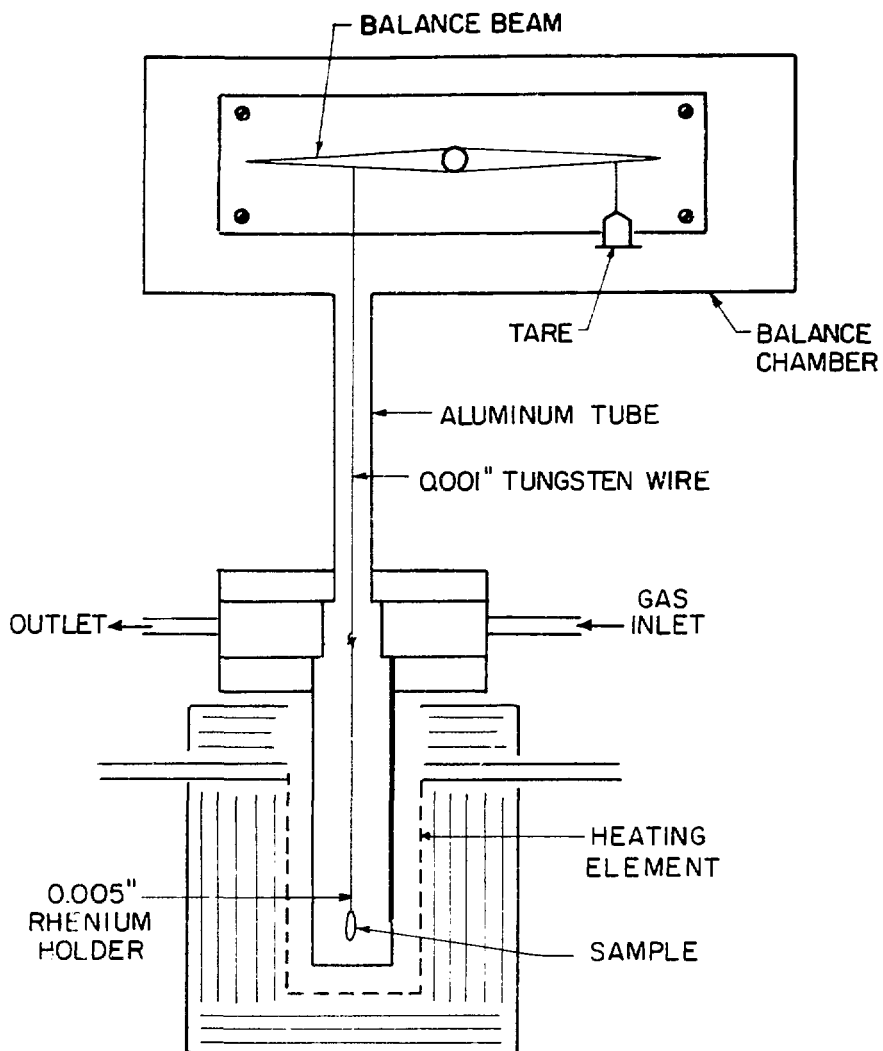
Figure 9. The thermobalance setup.

XBL 8010-6100

Figure 11. Photograph of the furnace with thermobalance.

from the balance beam to the end of the hangdown tube, a 0.001 in. thick tungsten wire was used which was thin and flexible enough to be straightened by the weight of the sample. Then a 0.005 in. thick rhenium wire was connected to it to hold the sample.

Since the continuous gas flow provided substantial noise to the balance it was necessary to use an extra stage noise filter. A second stage filter essentially eliminated noise from the output.

3.2.1.2 Gas Purifier

To reduce UO_2 the hydrogen had to be as free of H_2O as possible. For example at 1900°C, 10 ppm of $H_2^{18}O$ in H_2 would limit the thermodynamic capability of reduction to $O/U=1.975$.

To remove H_2O and other contaminants from H_2, the gas was passed through a liquid nitrogen cooled trap consisting of activated charcoal and a molecular seive.

3.2.2 Procedures for Reduction/Evaporation Tests

UO_2 specimens were essentially same in weight and shape as the ones used in the previous experiments. For the purpose of comparison, iron samples of similar geometry were tested, of which equilibrium vapor pressures are well known [29]. UO_2 samples were tested in argon and hydrogen, and for iron, helium and hydrogen were used. The balance was calibrated for each run.

3.2.2.1 UO_2 in Ar

(1) Pump out the entire system; The sample was degassed at 300°C
for 2 hrs at the same time. During the degassing step the
typical weight loss was approximately 0.1 mg for 1 gm sample.

(2) Fill the entire system with Ar and set the flow rate.

(3) Heat up to the predetermined temperature; measure the rate of
weight loss for different flow rates and temperatures.

(4) Cool down.

3.2.2.2 UO_2 in H_2

(1) Pump out the entire system.

(2) Fill the system with Ar and start flowing.

(3) Heat up to the predetermined temperature; measure the rate of
weight loss.

(4) Maintain the temperature until the rate reaches a steady state.

(5) Shut off Ar and switch to H_2; The temperature was changed
due to the difference in the properties of these two gases.
The voltage had to be lowered to maintain the temperature.

(6) Flow H_2 until the weight loss rate reaches a steady state.

(7) Cool down to 1000°C.

(8) Flush the system with Ar; It was necessary to cool down the
reduced UO_{2-x} in an atmosphere free of hydrogen because the
precipitated uranium would react with H_2 to form hydride,
which would result in a total destruction of urania.

(9) Cool down.

3.2.2.3 Iron Samples

Iron samples were tested in the streams of He and H_2. The same
procedure was taken as UO_2 except that lower temperatures were
employed.

3.2.3 Results and Discussion

3.2.3.1 UO_2 Vaporization in Argon

Table 3 shows the weight loss rates of UO_2 in argon streams at
three different temperatures and different flow rates.

Table 3. UO_2 Vaporization in Ar

$T^\circ K$	Flow Rate cc(stp)/sec	v cm/sec	$\dot{W}$ mg/min	κ_m	κ_m'
1340	20	13.8	$\simeq 0$	0	–
2173	3	3.9	0.009 ± 0.001	24.4	4.2
2173	10	11.1	0.110 ± 0.001	27.1	4.7
2173	20	22.2	0.014 ± 0.002	39.0	6.6
2273	20	23.3	0.043 ± 0.005	38.0	7.0

$\dot{W}$ = weight loss rate

T = temperature

κ_m = experimental mass transfer coefficient, defined by $J = \kappa_m P_{eq}/RT$

κ_m' = mass transfer coefficient calculated from theory

Sh = $\kappa_m l/0$

l = diameter of sample

D = diffusivity of $UO_2(g)$ in Ar

P_{eq} = equilibrium vapor pressure of UO_2

J = mass flux

Re = vl/v

v = velocity

v = kinematic viscosity

Sc = v/D

From the analogy between heat and mass transfer laminar boundary layer theory for a flat plate, the mass transfer coefficient k_m is predicted by:

$$Sh = 0.664 \ Sc^{1/3}Re^{1/2} \qquad . \tag{23}$$

As can be seen in Fig. 11, mass transfer of UO_2 vapor in argon was as much as six times faster than predicted. Using least squares fitting, the data at $2173°K$ are represented by: $Sh = 3.91 \ Sc^{1/3}Re^{(0.47\pm0.01)}$. The possible errors may be: (i) underestimation of diffusivity of $UO_2(g)$ in argon. (The transport properties estimated from theory [30] are given in Table 4.) (ii) flat plate boundary layer theory was not very accurate for a thick disk hung in a gas stream. (The effect of decreasing flow path length from the center to the periphery was small.) Nevertheless, the data still seem to follow the theoretical dependence on Reynolds number, as shown in Fig. 11.
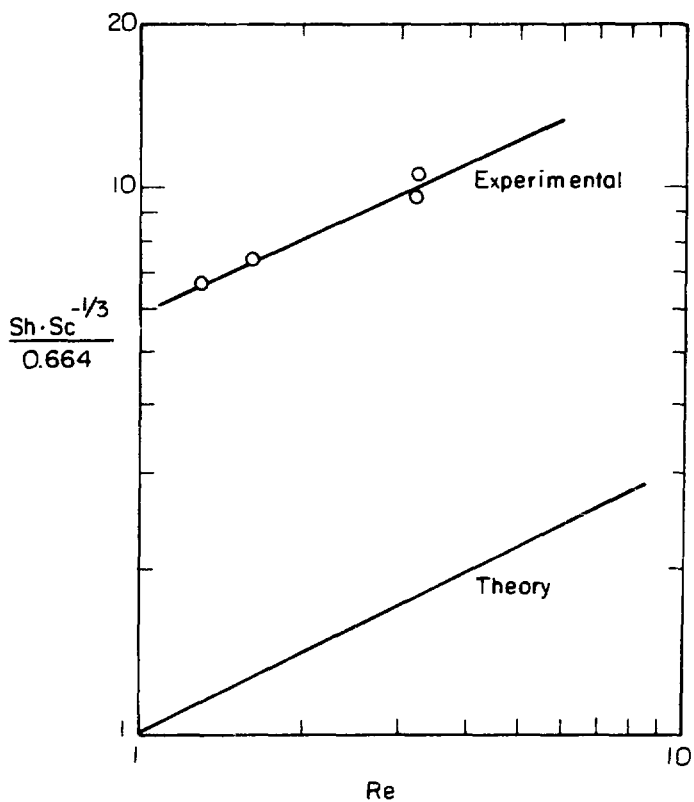
XBL 7712-6572

Figure 11. Comparison of UO$_2$ vaporization in argon with flat plate boundary layer theory for Reynolds number variations.

Table 4. Diffusivity and Viscosity of Ar and H_2

$T^\circ K$	D_{UO_2-Ar}, cm^2/sec	μ_{Ar}, Poise	$D_{UO_2-H_2}$, cm^2/sec	μ_{H_2}, Poise
2073	2.31	7.7 x 10^{-4}	12.53	3.2 x 10^{-4}
2173	2.48	7.8 x 10^{-4}	13.59	3.3 x 10^{-4}
2273	2.71	7.9 x 10^{-4}	14.54	3.4 x 10^{-4}

The effect of temperature on UO_2 vaporization can be estimated from the data in Table 3 at $2173^\circ K$ and $2273^\circ K$. From Eq. (23) and $J_{vap} = k_m P_{eq}/RT$ and $\dot{W} = JA$ where A = surface area of sample,

$$\frac{\dot{W}}{A} = k_m \frac{P_{eq}}{RT} \tag{24}$$

$$\text{or } \frac{\dot{W}T}{DSc^{1/3}Re^{1/2}} \propto P_{eq} \tag{25}$$

In Fig. 12, the temperature dependence of $\dot{W}T/DSc^{1/3}Re^{1/2}$ is compared with equilibrium vapor pressure curve. Least squares fitting yields a slope corresponding to a heat of vaproization $\Delta H_{vap} = 123.3 \pm 4.5$ kcal/mole which is in fair agreement with $\Delta H_{vap} = 143.1$ kcal/mole obtained from the equilibrium vapor pressure curve [31].

3.2.3.2 UO_2 Reduction in Hydrogen

Table 5 shows the results in H_2 streams.
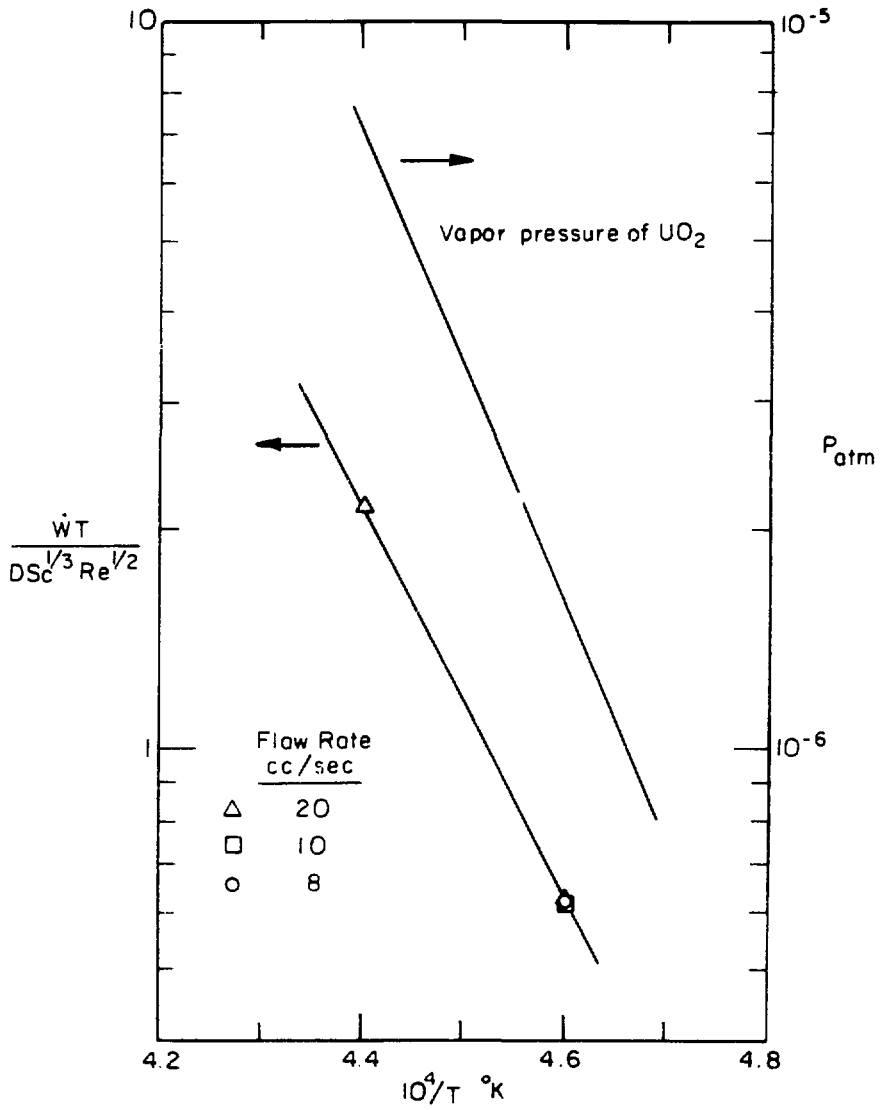
XBL 7712-6573

Figure 12. Temperature dependence of the UO₂ vaporization rate.

Table 5. UO_2 reduction in hydrogen.

$T^\circ K$	Flow Rate cc(STP)/sec	$\dot{W}$ in H_2, mg/min	$\dot{W}$ in Ar, mg/min	Expected $\dot{W}$ in H_2, mg/min
2173	10	0.011 ± 0.0005	$0.0\ 0 \pm 0.001$	0.021
2173	20	0.050 ± 0.0025	0.014 ± 0.002	0.029

Fig. 13 is a typical weight loss curve from thermobalance output in which one can see the sharp change of the slope after the argon stream was replaced by hydrogen.

Also shown in Table 5 are the weight loss rate in Ar for comparison. Using Eq. (23), the ratio of κ_m in H_2 to κ_m in Ar is estimated to be ~2.1 at the same temperature and flow rate, and the weight loss rates due to pure evaporation are listed as "Expected $\dot{W}$ in H_2" in the table. However, the data at a flow rate of 10 cc/sec show a slower rate than expected, especially considering the contribution of reduction. This is believed to be experimental error. Another possibility is that the rate 0.011 mg/min was measured before steady state was reached. For a flow rate of 20 cc/sec, the weight loss rate $0.050 - 0.029 = 0.021$ mg/min could be attributed to the reduction of UO_2 by H_2. At this rate, UO_2 could have been reduced to $UO_{1.977}$ in an hour, assuming that the vapor pressure was independent of stoichiometry within this range. This rate of reduction was significant and may have been mass transfer-limited (rather than limited by a surface chemical reaction or solid state diffusion of oxygen in the UO_{2-x}).
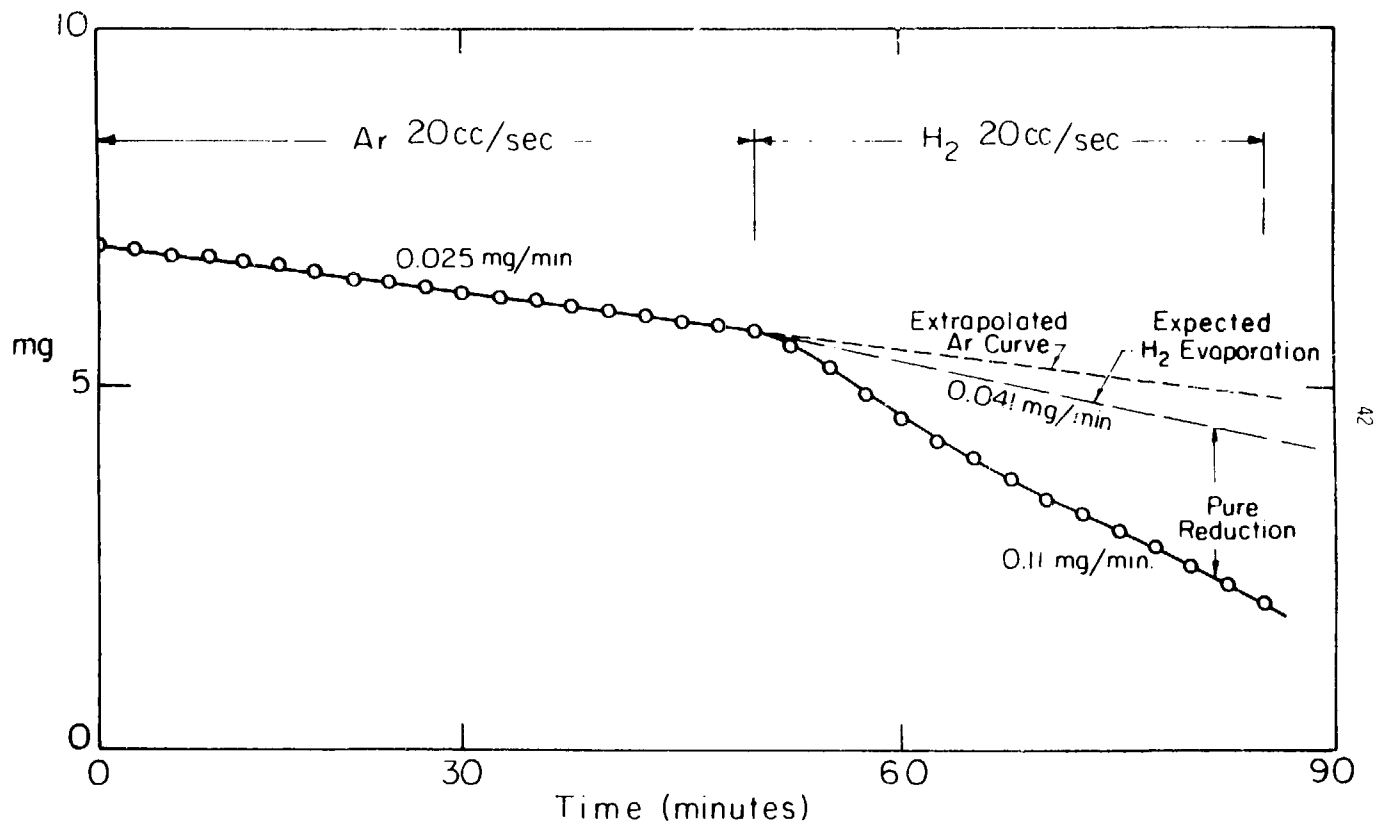
Figure 13.   Typical weight loss data for UO_2 in flowing argon and hydrogen.   XBL 7712-6574

3.2.3.3 Iron Vaporization

Iron evaporation results are shown in Table 7. Fig. 14 shows that mass transfer was 2-3 times higher than expected from the theory. Using least squares fitting, the experimental data can be represented by: $Sn = 0.3 \, Sc^{1/3} Re^{(0.115\pm0.3)}$. Diffusivities of Fe in H_2 and He calculated by theory [30] are tabulated below:

Table 6. Diffusivity and Viscosity of He and H_2

| $T^\circ K$	D_{Fe-H_2},cm^2/sec	D_{Fe-He},cm^2/sec	μ_{H_2},Poise	μ_{He},Poise
1693	14.48	13.76	2.7×10^{-4}	6.3×10^{-4}
1773	15.75	14.88	2.9×10^{-4}	6.5×10^{-4}

The dependence of the Sherwood number on the Reynolds number does not agree with the value of 0.5 predicted by laminar flat plate boundary layer theory. This discrepancy may be due to the sensitivity of the hydrodynamics to slight misalignment of the hanging specimen from the vertical axis. Note also that the magnitude of the discrepancy between theory and experiment is a factor of ~2 instead of ~6 for UO_2.

The heat of vaporization $\Delta H_{vap} = 91.2 \pm 32.1$ kcal/mole was obtained from Fig. 15, which is in good agreement with $\Delta H_{vap} = 90.1$ kcal/mole obtained from the equilibrium vapor pressure curve [29].
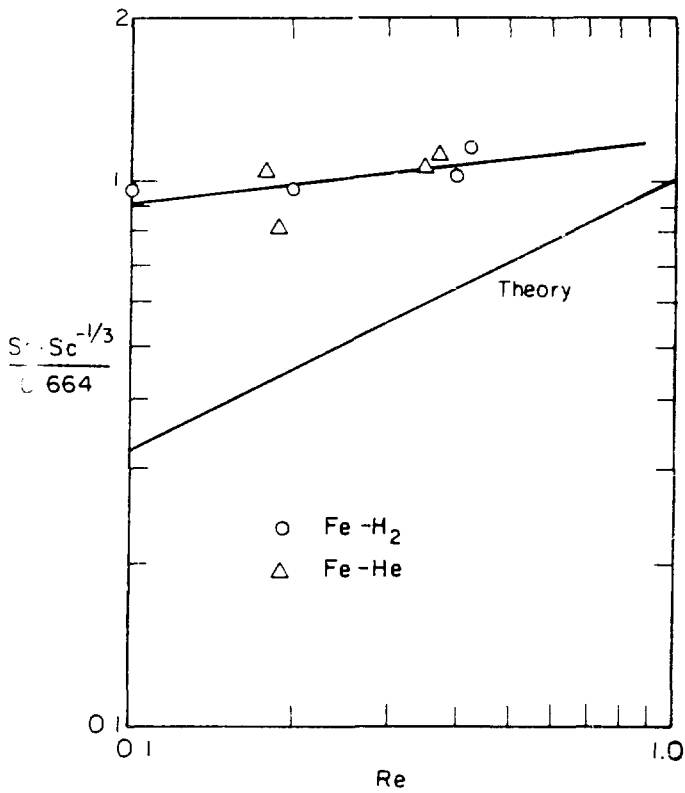
XBL 7712-6575A

Figure 14. Comparison of iron vaporization in hydrogen and in helium.

45
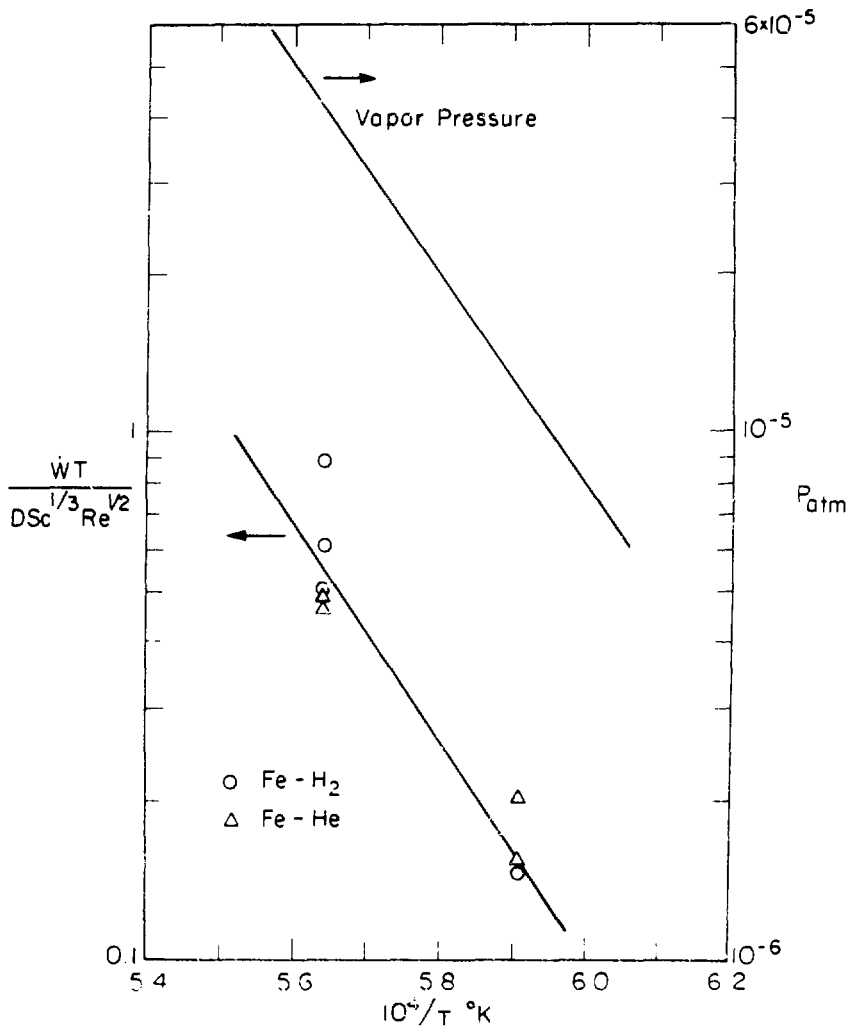
XBL 7712-6576

Figure 15.   Temperature dependence of iron vaporization.

Table 7. Fe Vaporization in H_2 and He

Conditions				H_2			He		
T^*K	P_{eq}, atm	Flow cc/sec	v cm/sec	$\dot{W}$ mg/min	κ_m cm/sec	κ_m' cm/sec	$\dot{W}$, mg/min	κ_m cm/sec	κ_m' cc/sec
1486	–	20	13.96	≈ 0	–	–	–	–	–
1693	1.21×10^{-5}	10	7.95	–	–	–	0.012 ± 0.003	22.9	9.1
1693	1.21×10^{-5}	20	15.90	0.013 ± 0.004	24.8	13.63	0.013 ± 0.002	24.8	12.9
1773	4.12×10^{-5}	5	4.16	0.038 ± 0.003	22.2	3.64	–	–	–
1773	4.12×10^{-5}	10	8.33	0.038 ± 0.007	22.2	7.30	0.030 ± 0.005	17.5	9.3
1773	4.12×10^{-5}	20	16.65	0.041 ± 0.005	23.6	14.59	0.039 ± 0.002	22.8	13.6

3.3 Reduction of UO_2

Uranium oxide at elevated temperature exists as a single phase over a broad range of stoichiometry (see Fig. 1). In the oxygen deficient region, this extends down to O/U ratio of about 1.46 at a monotectic temperature of 2425°C.

As was mentioned earlier, hypostoichiometric urania can be prepared by reduction of UO_2 in hydrogen. In this technique the purity of hydrogen is essential. The ultimate stoichiometry is limited by the oxygen potential of the stream (see Fig. 3).

3.3. Apparatus

The thermobalance was not needed in the UO_2 reduction step. From the previous experience a standard procedure was established.

Since hydrogen free of oxygen and water is essential to the capability of reduction, in addition to the activated charcoal fil.ed liquid nitrogen trap, H_2 was passed through an oxygen getter con- sisting of copper turnings at 650°C. This served to remove any oxygen in the hydrogen stream by oxidation of copper. Copper turnings were contained in a 1-1/4 in. O.D., 10 in. long stainless steel tube which was heated from outside. On some occasions fused titanium lumps were used as the getter instead of copper.

3.3.2 Procedure for Reducing UO_2

One set of matched UO_2 wafers (one $U^{16}O_2$ and the other $U^{18}O_2$) that had gone through the oxygen exchange steps was placed in the furnace together. The rhenium rig used in the oxygen exchange step was used here. The two wafers were separated as far as possible in order to prevent (or minimize) premature isotope exchange via vapor pnase

transport. Also present was another identical UO_2 wafer, which was to serve the purpose of stoichiometry determination after the reduction. This was necessary because a nondestructive method of stoichiometry determination was not available.

(1) Pump out the entire system; samples were simultaneously degassed at $300°C$. This time all tubing was baked as were the molecular seive and the activated charcoal-filled liquid nitrogen moisture trap. This step was to remove any H_2O inside the tubing. It was most essential when the system had been previously exposed to H_2O-H_2 mixture.

(2) Fill the system with helium; oxygen-free helium was used. Flush the system for 30 mins.

(3) Heat up the copper getter to $650°C$.

(4) Start heating up the furnace to $1000°C$; Again, slow heatup was essential to prevent cracking of the UO_2. Approximately 30 mins. were requied.

(5) Shut off helium.

(6) Flow hydrogen at 20 cc/sec; Hydrogen was passed through the liquid nitrogen trap and the copper getter.

(7) Raise the temperature to $1900 \sim 2000°C$; Normally 2-4 hrs. were required to substantially reduce UO_2.

(8) Stop flowing hydrogen and anneal the samples for 2 hrs.; this was to eliminate any oxygen concentration gradient in the samples.

(9) Cool down the temperature to $1000°C$.

(10) Pump out the entire system; Before cooling down to room
     temperature the system had to be absolutely free of hydrogen
     to avoid hydriding the precipitated uranium which would lead
     to a complete destruction of the samples.

(11) Fill the system with helium and flow.

(12) Cool down to room temperature.

3.3.3 Results

Shown in Table 8 are several results of reduction. The degree of
reduction was controlled by the reaction time and temperature.

Table 8. Typical Results of Reduction in H_2 Flow.

$T^\circ C$	H_2 cc/sec	time, hrs	Final O/U poly. crystal	single crystal
1850	20	1	1.972	–
1850	10	1	1.970	–
1850	20	2	1.954	1.970
1950	20	2	1.951	–
1950	20	4	1.955	–
1950	20	4	1.954	–
2000	20	4	1.950	1.953
2000	20	4	1.955	1.950
2020	20	4	1.948	–
2040	20	4	1.945	1.944
2040	20	4	1.951	–

The stoichiometries were measured by a thermogravimetric method
which will be described in the next chapter.

Apparently the stoichiometry approached 1.95 rather rapidly and reached a plateau. It looks, however, as if higher temperatures may lead to lower stoichiometries, which is consistent with the fact that at higher temperature the equilibrium oxygen potential is higher (see Fig. 3).

However, temperatures above 2050°C were not imposed because of a severe distortion of the shape of the sample due to the extremely high vaporization rates. The reduced samples were not to be ground or polished again because of the possibilities of contamination and change in stoichiometry. Therefore, a severe distortion in the shape of the samples could not be tolerated.

Both single crystal and polycrstalline samples showed similar stoichiometries after the reduction in similar conditions. At this stage this was interpreted as (1) oxygen diffusion in UO_2 was not rate controlling or (2) reaction had reached equilibrium.

At the conditions of T=2000°C and H_2 flow of 20 cc/sec for 4 hrs, approximate stoichiometries of 1.95 could be consistently obtained.

Shown in Fig. 16 is a photomicrograph of a reduced sample. The uranium metal precipitates are immediately visible (bright areas); many of them associated with voids. Using EDAX (Energy Dispersive X-ray Analysis), the bright areas were confirmed to be uranium metal. Figure 17 shows one of the uranium precipitates under SEM.

The reduced wafers that were to be used in diffusion experiment already had gone through oxygen exchange steps described previously. This process, which took ~40 hrs., combined with 4 hrs. reduction at high temperature, yielded very large grains, approximately 200 microns. Figures 18 and 19 show the morphologies of $U^{16}O_{2-x}$ and $U^{18}O_{2-x}$ specimens, respectively. As expected they show approximately same grain size.

3.4 Stoichiometry Determination

3.4.1 Survey of Methods

There are a number of different methods for measuring the stoichiometry of urania. Methods commonly used are:

1. X-ray diffraction [32]: The lattice parameters are correlated with the O/U ratio. By measuring this parameter the stoichiometry is obtained.

2. Solid State Electrolytic Cell [33]: High temperature galvanic cells using Ni-NiO mixture and heavy metal oxides (TnO_2, UO_2, etc.) are utilized. The equilibrium oxygen potential can be measured by the emf generated between the two electrodes.

3. Gas Equilibrium Method [34]: Using appropriate gas mixture of $CO-CO_2$ or H_2O-H_2 the specimen is brought to stoichiometric UO_2 and the total accumulated change in the ratio of the CO/CO_2 or H_2O/H_2 during this process is recorded to calculate the original stoichiometry.

4. Thermogravimetric Method [35]: By measuring the weight change of the specimens when they are brought to a known, standard stoichiometry (UO_2 or U_3O_8), the original stoichiometries can be obtained.

50 μm
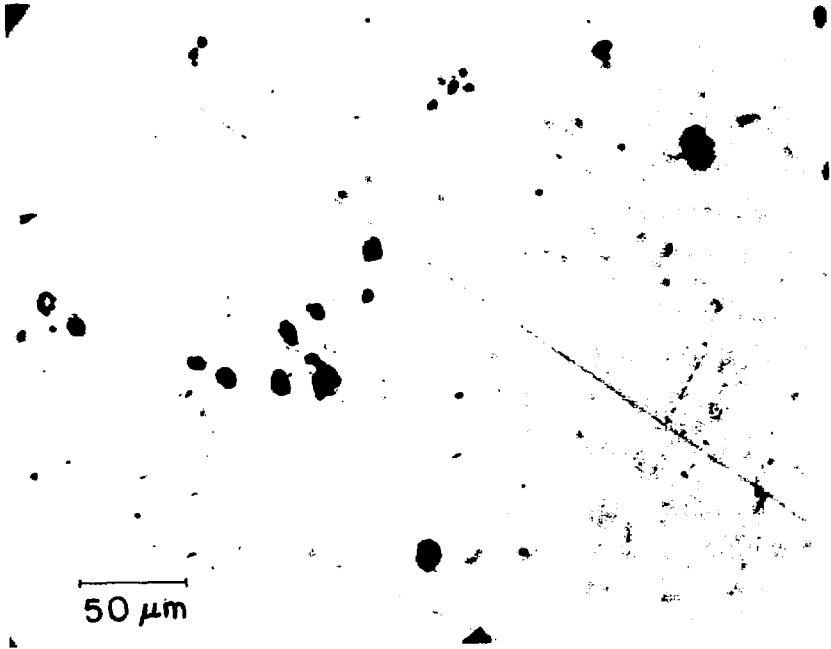
XBB 800 13463

Figure 16. Photomicrograph of the reduced urania. Bright spots
are the uranium metal precipitates.
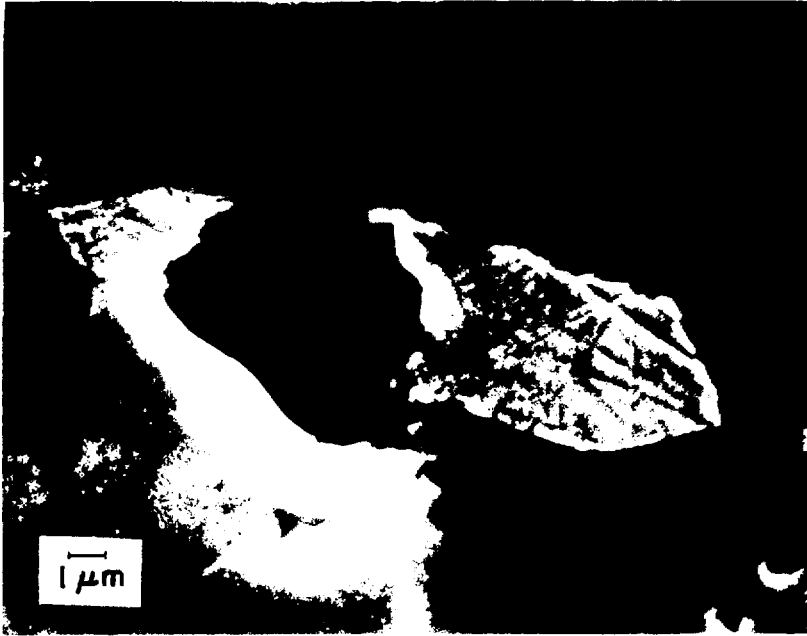
XBB 800 13489

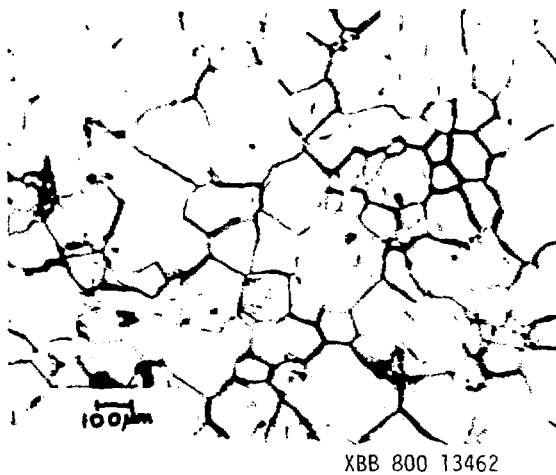Figure 17.   Photomicrograph of the uranium precipitates under SEM.

54

XBB 800 13462

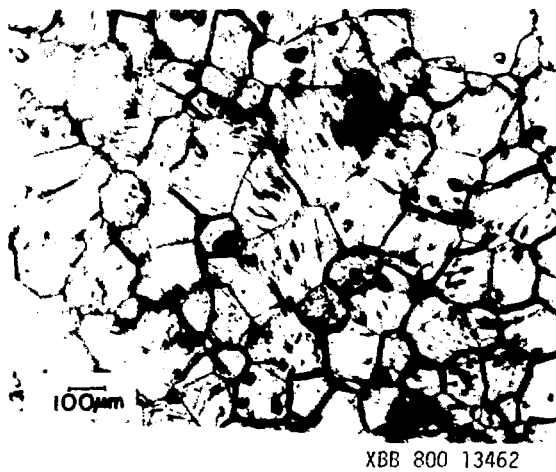Figure 18. Photomicrograph of the $U^{16}O_{2-x}$ surface.

XBB 800 13462

Figure 19. Photomicrograph of the $U^{18}O_{2-x}$ surface.

Of all these methods, the thermogravimetric method is the most convenient and reliable for routine experiments. Also it was readily available since the system was equipped with thermobalance.

Since there was a substantial amount of vaporization at high temperature, the degree of reduction could be measured directly by the total weight change during the reduction step. This problem was overcome simply by having another piece of UO_2 present during the process and subsequently oxidizing it back to UO_2 at low temperature while measuring the weight gain, from which the stoichiometry can be calculated by:

$$\frac{O}{U} = 2.0 - \frac{270}{16} \quad \frac{W_f - W_i}{W_f} \tag{25}$$

where W_i and W_f are weight of the sample before and after the reaction, respectively.

3.4.2 Procedure for Stoichiometry Measurement

The atmospheric conditions for this oxidation were almost the same as the ones used in the oxygen exchange step described previously. Here, normal water was used and in order to minimize the chance of vaporization, lower temperatures were employed (~1300°C rather than 1500°C). At these temperatures the amount of evaporation was negligible, yet reaction was fast enough. As in the oxygen exchange procedure, the water was kept at 7.5°C, which would yield an oxygen potential of -105 kcal/mole at 1300°C.

Sometimes the specimen surface spalled due to a sudden violent reaction between uranium precipitation and H_2O, which caused a large weight change. Therefore, the specimen had to be contained in a rhenium basket so that the small particles were not lost from the weight measurement. This basket in turn was suspended from the thermo-balance to follow the weight change continuously throughout the experiments. Although spallation did not happen very often, the precautions were taken each time.

Before and after the reaction, the specimen was weighed outside the system using the Mettler microbalance to compare with the output of the thermobalance. Most of the time those two readings were in good agree-ment. However, the calibration of the thermobalance seemed easy to disturb when a sudden large force was exerted, for example a sudden change in flow rate. Thus, whenever there were significant discrepan-cies between those two readings, the Mettler's reading overruled that of the thermobalance. The main function of the thermobalance was to provide the indication that the reaction was completed by showing a steady weight. The following is the detailed procedure:

1) Measure   weight of the specimen before loading.

2. Pump ti   or   system and degas the specimen.

3) Fill the sy   ium.

4) Flow heliu   cc/sec.

5) Heat up to $1000°C$; The reduced samples should not be exposed to hydrogen at low temperature.

6) Shut off helium.

(7) Flow nydrogen 10 cc/sec.

(8) Heat up to $1300^{\circ}C$.

(9) Start flowing H_2O-H_2 5 cc/sec.

(10) Ooserve the weight reaches a steady state.

(11) Flow nydrogen 10 cc/sec

(12) Cool down to $1000^{\circ}C$.

(13) Snut off nydrogen.

(14) Flow helium 10 cc/sec.

(15) Cool down to room temperature.

(16) Shut off nelium.

(17) Take out the specimen and measure the final weight.

Since the balance was extremely sensitive, the valve operations and flow rate cnanges gave considerable perturbations. Also for different conditions (temperature, gas species, flow rate), the readout was different even though the weight of the sample remained unchanged. Changes occurred because (1) for different gas species and/or flow rates the buoyancy and skin friction forces are different and (2) for different temperatures the brightness in the balance chamber changes due to the radiation and this contributes to a change in the readout because the balance has a photoelectric tube the current of which is directly proportional to the readout. Therefore, it was essential to compare the readout at identical conditions (i.e., at the same temperature, same gas species, and same flow rate), to obtain a true weight cnange of the specimen. It was also essential to take the reading after the system reached a steady state following each perturbation.

To satisfy these requirements the weight increase was calculated by comparing the weights at steps (9) and (10), (11) and (8), (12) and (17), (14) and (15), and (15) and (4). These points are depicted in Fig. 20. In most cases these values were in agreement to within ±0.005 mg. An average of these values represented the thermobalance measurement.

In order to make sure that the rhenium wire and basket holding the specimen did not react with H_2O-H_2 during the process, a dummy experiment was performed without any sample in the basket. In the basket was a piece of rhenium foil of approximately the same weight as the UO_{2-x} specimen. The test consisted of exactly the same steps as the actual stoichiometry determination, except that the temperature was raised from $1300^\circ C$ to $1500^\circ C$ gradually in the H_2O-H_2 stream. No weight change was observed through $1500^\circ C$. This proved that the conditions for the stoichiometry determination were inert to rhenium and all the weight change observed could be attributed to the reaction of UO_{2-x} specimen with H_2O.

Shown in Fig. 20 is a typical output of the thermobalance during the experiment. Each step of the procedure was marked by a numbered arrow. Step 3 shows a sudden huge perturbation when the pre-evacuated system is filled with helium. Similar, but smaller, spikes are seen on many other occasions whenever there were valve operations or changes in the flow rate. Also observed is a difference of ~0.4 mg in readout before and after filling the system with helium, although the weight of the specimen should have remained unchanged. This change was due to the buoyancy force exerted to the whole balance system by helium gas.
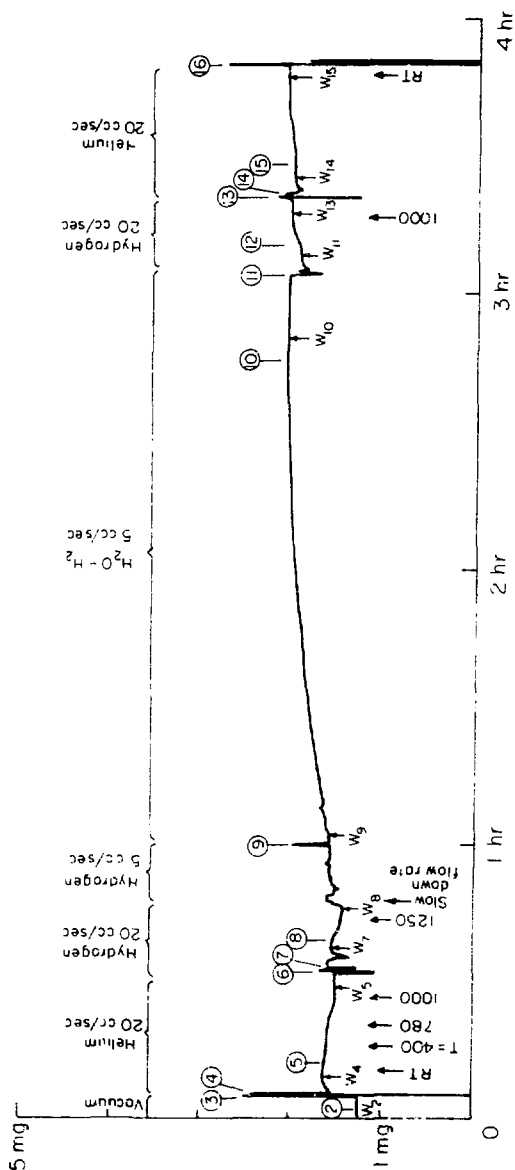
59

Figure 20. Typical thermobalance output during the stoichiometry determinations.

XBL 8010-6095

Also, as the temperature increased from room temperature to $1000°C$ the readout decreased by ~0.15 mg due to the radiation into the balance chamber.

Before feeding H_2O-H_2, it was verified that the weight remained constant under steady H_2 flow. This test was necessary to make sure that (i) evaporation of the sample was negligible and (ii) all the weight increase in the H_2O-H_2 atmosphere could be attributed to the reaction of H_2O and UO_{2-x}.

In the example of Fig. 20 it took 1.5 hrs to complete the reaction. The time required for the reaction varied from 1.5 hrs to 3 hrs in most cases. It is very likely that this range was due to the different geometries of the samples.

Table 9 shows the weight increase measured at different conditions. As mentioned earlier, for each measurement the conditions of comparison were identical.

Table 9. Weight increase measurements at different condtions.

W_j-W_k	gas	Condition: flow cc/sec	$T°C$	ΔW mg
$W_{10}-W_9$	H_2O-H_2	5	1250	0.475
$W_{11}-W_8$	H_2	10	1250	0.475
$W_{12}-W_7$	H_2	10	1000	0.48
$W_{14}-W_5$	He	10	1000	0.48
$W_{15}-W_4$	He	10	room temp.	0.475
W_f-W_i	air	0	room temp.	0.485

Weights $W_i = 0.178370$ gm and $W_f = 0.178855$ gm were measured by the Mettler microbalance for this example. The measured weight

increases in Table 9 are in good agreement with the measurement by Mettler microbalance. Using a 0.485 mg increase, the initial stoichiometry was calculated from Eq. (26) to be 1.954.
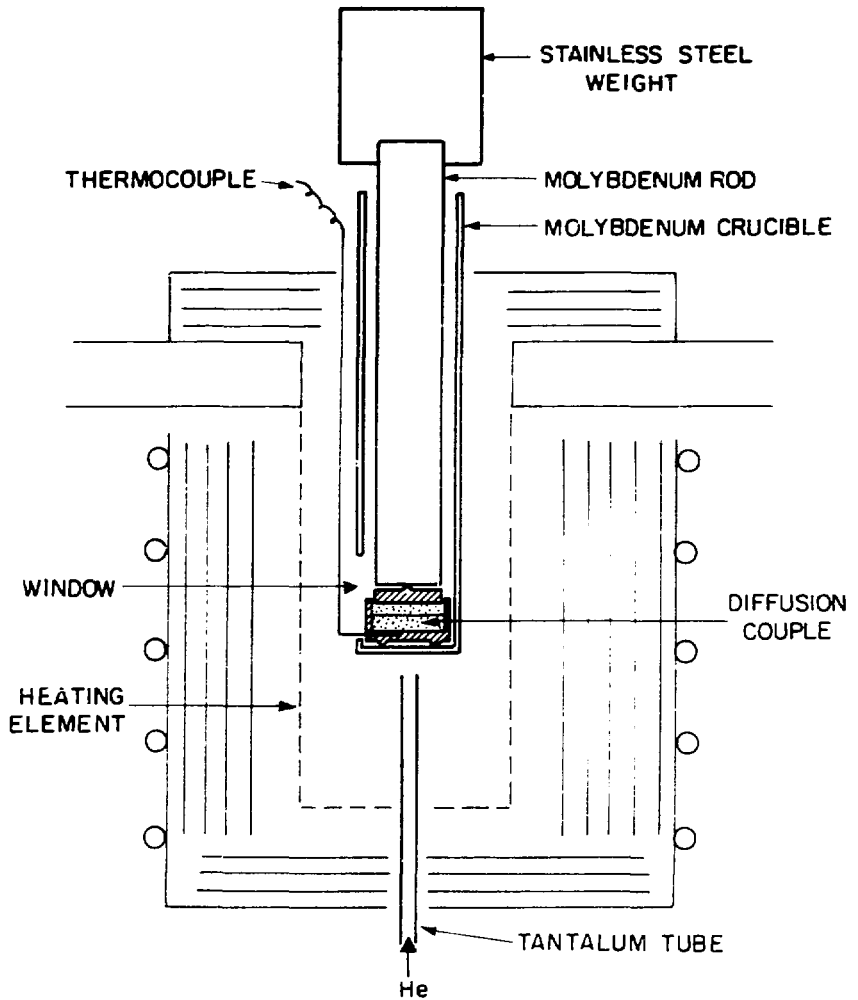
4. DIFFUSION EXPERIMENT

4.1 Apparatus and Procedure

Following the preceding steps, two identical nypostoicniometric UO_{2-x} wafers (one with ^{18}O and tne other normal) were prepared for each diffusion experiment. Tnese two matched wafers were put togetner with a uranium foil 0.003 in. tnick in between. Snown in Fig. 21 is tne experimental setup. Experiments were performed in a glass belljar filled with high purity helium. Tnroughout the experiment tne nelium flowed continuously from underneatn the sample to keep tne surrounding atmospnere as clean as possible.

Tne furnace was heated by a tungsten mesn heating element of 3 in. diameter and 6 in. nigh. The diffusion couple was positioned in the center of the neating element to establish as uniform a temperature as possible in the diffusion couple. Since the samples were approximately 1 mm thick, wnich is very small compared to tne size of the heater, it was assumed that tne temperature was uniform tnroughout the diffusion couple.

The diffusion couple was enclosed by a molybdenum crucible of 0.5 in. I.D. (see Fig. 22). It was necessary to make the crucible wide enougn to accommodate the thermal expansion of urania.

In order to oromote good contact between the two wafers and to minimize tne thickness of the liquid uranium layer, the diffusion couple was put under compression. This was achieved by a weight on top of tne molybdenum crucible.

Figure 21. Diffusion experiment setup.
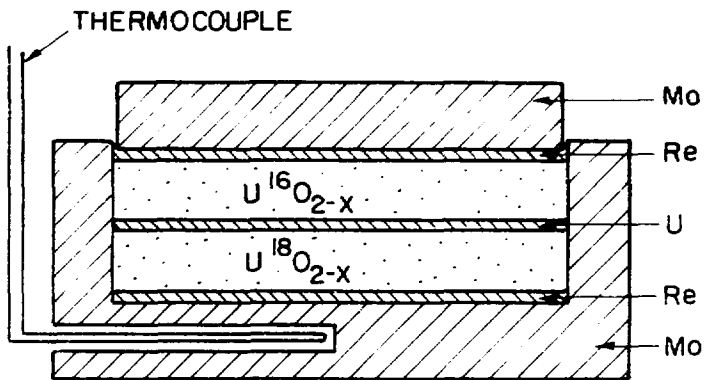
XBL 8010-6087

XBL 8010-6086

Figure 22. Diffusion couple arrangement.

Temperature was measured by a W3%Re-W25%Re thermocouple the hot junction of which was placed in the center of the molybdenum crucible (see Fig. 22). The distance between the junction and the end of UO_{2-x} wafer was less than 1/16 in. The thermocouple was connected to a digital indicator from which the temperatures were read directly. In order for the thermocouple to respond quickly to the temperature changes, unsheathed bare wire thermocouple was used.

Prepared samples were stored in an inert gas or vacuum until they were used in the diffusion experiment.

The following steps were taken for each run:

(1) Pump out the entire system.

(2) Heat up to 400°C to degass the system for one hour.

(3) Fill the system with high purity oxygen-free helium.

(4) Flow helium at 20 cc/sec.

(5) Slowly heat up to 1100°C; Slow heatup was essential to prevent the samples from cracking. Since the uranium remained solid up to the melting point of 1132°C, it acted as a barrier to the premature diffusion.

(6) Rapidly heat up to the desired temperature; Once the uranium melted, diffusion through it would occur. Therefore, it was necessary to reach the temperature as quickly as possible. It usually took 40 sec.-2 mins., which was short compared to the total annealing time.

(7) Maintain the temperature for a predetermined time period; For the first experiment, the diffusion coefficient had to be guessed in order to determine the appropriate annealing time.

From the result of this first experiment, diffusion coef-
ficients at other temperatures could be estimated and the
annealing time which would yield an appropriately developed
diffusion profile was determined. The criteria were that the
time should be long enough for diffusion to penetrate at least
half of the thickness, yet no more than 2/3 of the thickness.
By having a less than fully penetrated diffusion profile, the
original ^{18}O concentration on both sides of the diffusion
couple could be checked. This is discussed in greater detail
in the next section.

(3) Turn off the power supply to cool the couple as quickly as
possible; Since sintering of the two wafers could occur in
some contact areas of the sample, diffusion could take place
even below the melting point of uranium. Time required to
reach 1100°C was measured, which was also short compared to
the overall operation time.

After each run, the couple was taken out and was cut in half using
a low speed diamond saw. Each half was mounted in a copper filled
conductive thermosetting epoxy and polished to 5 micron grade using
diamond paste.

4.2 Sample Analysis and Results

$^{18}O/(^{18}O+^{16}O)$ profiles were determined by Hanford Engineering
Development Laboratory and Argonne National Laboratory using ion micro-
probe mass analyzer (IMMA). The basic operating principles of IMMA are
described elsewhere [36,37]. Basically, an ion beam is accelerated to
an adjustable focal spot on the sample surface and the sputtering ions

are analyzed by mass spectrometer. This technique was used by Marin
et al. [1] and Contamin et al. [3] for urania and by Valencourt
et al. [37] for porous UO_{2+x}.

For the present analysis an $^{28}N_2^+$ primary beam was used in 15-20 kv
accelerating potential. The area analyzed was about 5x6 microns for
each spot. Each area was sputter cleaned for 30 seconds before
collecting data to eliminate any surface effects.

Since H_2O also has mass 18, it is indistinguishable from ^{18}O
in the mass spectrometer. Therefore, water had to be avoided in
grinding and polishing the samples and they had to be degassed in a
high vacuum ($5x10^{-9}$ torr) for 2-3 days before each analysis. Also
samples were stored in vacuum after experiments and shipped in a small
leak-tight stainless steel containers filled with slightly pressurized
helium.

Experiments were conducted at eight different temperatures in the
range 1257 - 1597°C, each of them corresponded to stoichiometries in
the range of 1.993-1.955 following the lower phase boundary. An
empirical equation developed by Fryxell et al. [38] was employed to
determine the stoichiometries of the oxide in the two phase region:

$$\ln x = 3.078 - 12675/T°K \tag{27}$$

Shown in Table 10 are $(O/U)_0$, the stoichiometries of the samples
used in each experiment, annealing temperatures, and (O/U), the
stoichiometries of the oxide phase in the two phase region
corresponding to each temperature.

Table 10. Experimental temperatures, stoichiometries, initial ^{18}O compositions of the two wafers, and diffusion times.

RUN	T°C	$(O/U)_0$	(O/U)	^{18}O (%) by IMMA enriched wafer	normal wafer	original ^{18}O enrichment (%)	t_1 mins.	t_2 mins.	t_0 mins.
1	1190	1.970	1.993	70.9	1.2	71.5	1.0	1.0	340
2	1257	1.973	1.990	70.6	2.2	73.5	1.3	1.4	180
3	1330	1.954	1.985	70.0	0.3	72.3	0.8	0.8	20
4	1400	1.955	1.980	33.6	4.9	40.1	2.2	1.8	45
5	1400	1.975	1.980	54.1	2.1	61.5	3.0	1.5	30
6	1490	1.945	1.970	45.7	1.4	46.0	2.5	2.2	50
7	1530	1.948	1.965	47.1	2.1	51.2	2.1	2.0	35
8	1565	1.948	1.960	44.3	1.4	48.4	2.5	2.5	20
9	1597	1.945	1.955	45.2	1.5	47.9	3.0	2.3	20
10*	1330	1.950	1.985	61.0	4.9	69.8	1.6	1.5	45
11*	1400	1.956	1.980	58.1	5.8	65.2	2.2	1.8	45
12*	1490	1.944	1.970	58.7	2.1	65.0	3.0	3.0	28
13*	1565	1.950	1.960	65.1	2.7	--	2.5	2.5	15

*Single Crystals

In Fig. 23 the experimental points are depicted in the phase diagram. In order to make sure that the experimental points were in the two phase region, annealing temperatures were kept at least $50°C$ below the two phase boundary.

Calculation showed that under these conditions the effect of liquid phase on diffusion in the oxide is insignificant.

Shown in Figs. 24-37 are normalized profiles of $^{18}O/(^{18}O+^{16}O)$ analyzed by IMMA. For normalization of the raw data it was imperative to have correct values of original isotopic concentrations on both sides of the diffusion couple. Although the isotopic enrichment had been measured from weight increase after the oxygen exchange step, it was essential to confirm these measurements because any error in this value was directly passed along to the diffusion coefficient calculations. Since the wafers had gone through a high temperature reduction step, it was suspected that the original enrichments may have been altered by vapor phase isotope transport.

This could be verified by comparing the original isotopic enrichment with the IMMA data near the end of the wafer where diffusion had not yet penetrated. From the unnormalized IMMA data, it was obvious that in every experiment at least one third of the wafer had not been affected by diffusion. In some of the samples No. 3, 4, 10, 11, 12, more than half of the wafer was unchanged. Average values of these unchanged, flat profile regions are tabulated in Table 10. Also shown in the table are ^{18}O original enrichment values calculated from weight increase.
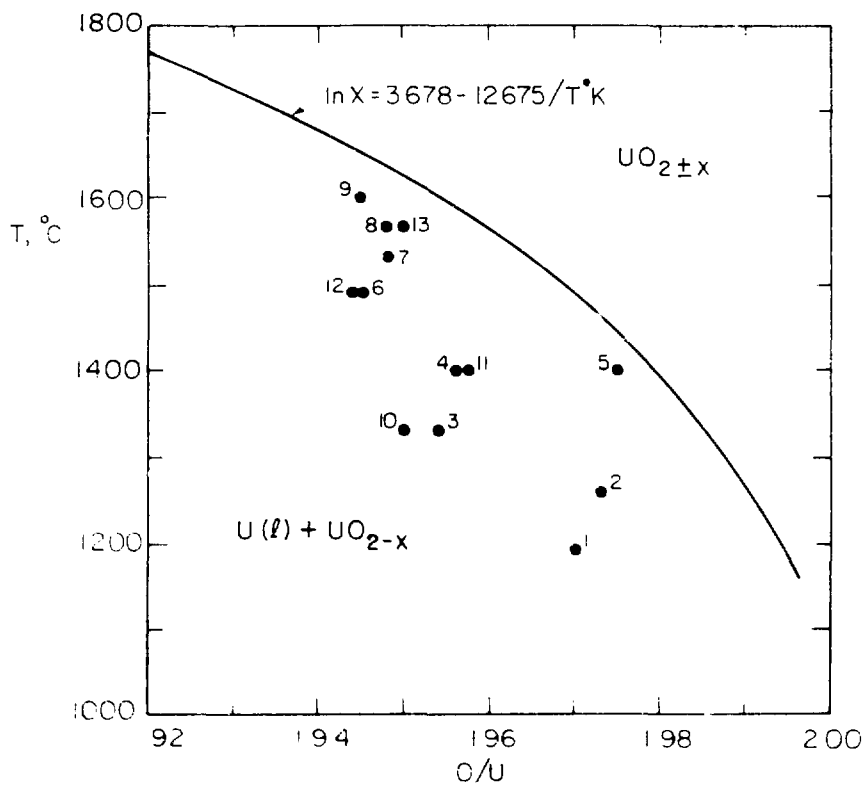
Figure 20. Experimental points in phase diagram.

IMMA data near the ends of $U^{16}O_{2-x}$ wafers showed substantially higher values of ^{18}O concentration (1-5 percent) than natural abundance (0.2 percent), which is easily detectable by IMMA (see Table 10). Yet, the profiles were also flat at least up to one third of the thickness, i.e., the maximum depth of diffusion penetration was two thirds of the thickness, i.e., the overall ^{18}O profiles were symmetric in every experiment. This implies that the ^{18}O concentrations were already higher than natural abandance in $U^{16}O_{-x}$ wafers even before the diffusion anneal. The immediate explanation is that there had been oxygen exchange between the two wafers through the vapor phase during the 4 hours of reduction at high temperature. This interpretation was strengthened by the fact that the sum of average values of both sides of the diffusion couple were close to the original enrichment (see Table 10). Based on this interpretation, the two ^{18}O fraction on the sides of the diffusion couple away from the interface obtained by IMMA were used for normalization of the data (see the definition of δ in Eq. (1)).

Experiments 10 through 13 are on single crystals.

In most experiments two different lines perpendicular to the interface were probed in order to average out any difference in the ^{18}O profiles. They were marked as triangles and squares in the Figs. 24-37. First one was usually near the center and the other was near half way to the edge from the center. Each position of the lines was carefully chosen under the microscope in such a way that the line of probe would not cross any voids or cracks which would cause IMMA to pick up values from different planes. As can be seen, the profiles of the two traverses were very close to each other in most experiments.
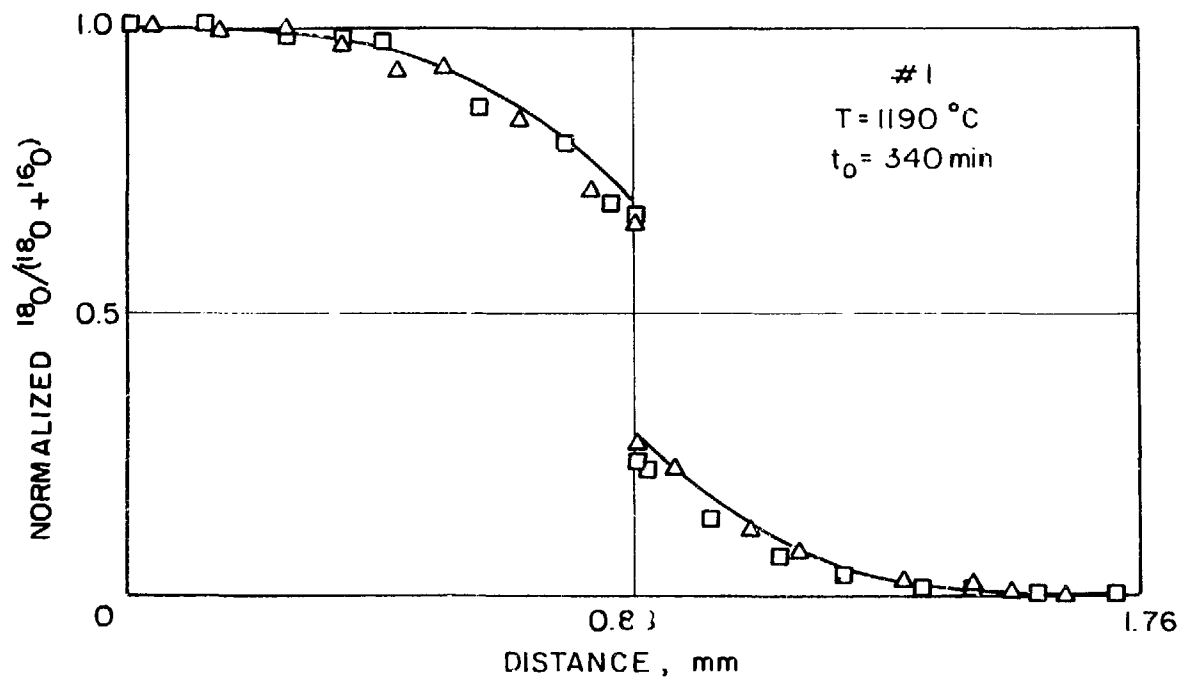
XBL 8010-6103

Figure 24. Normalized profile of ^{18}O concentration. Squares and triangles are for traverses near the center and near half way to the edge from the center, respectively.
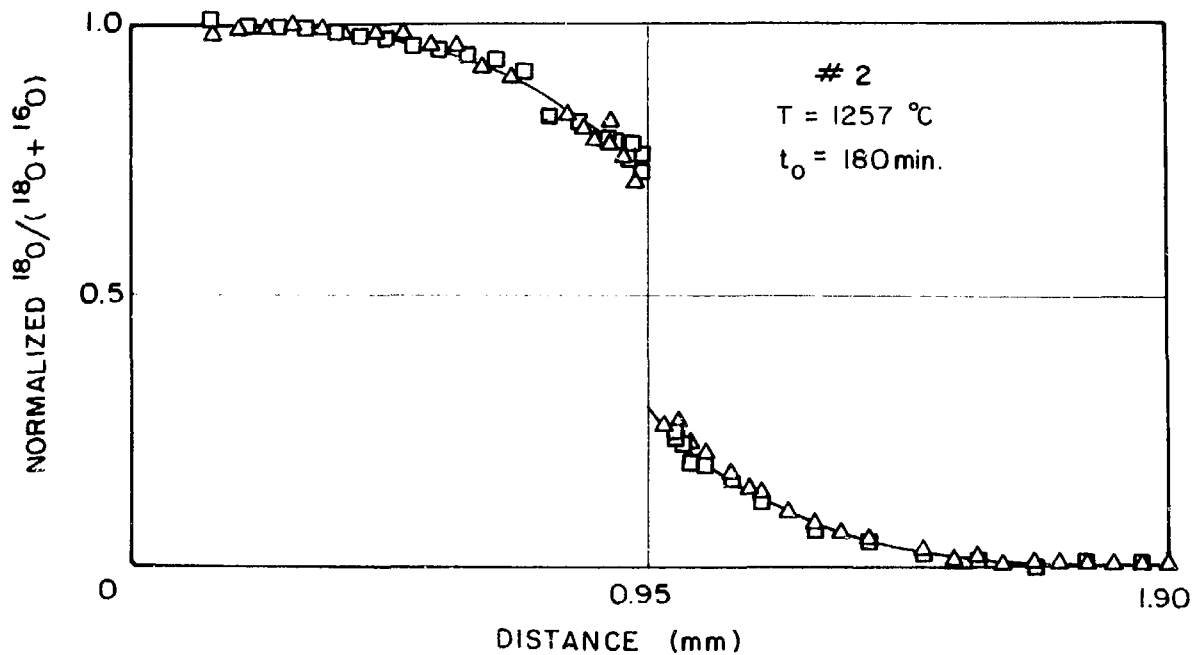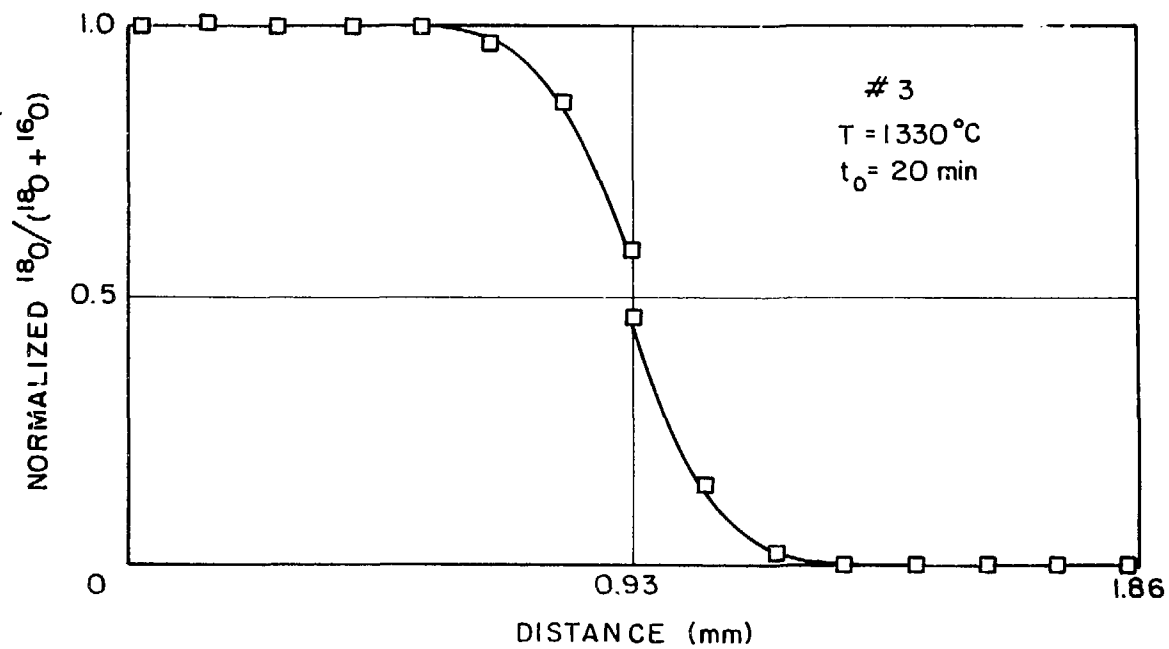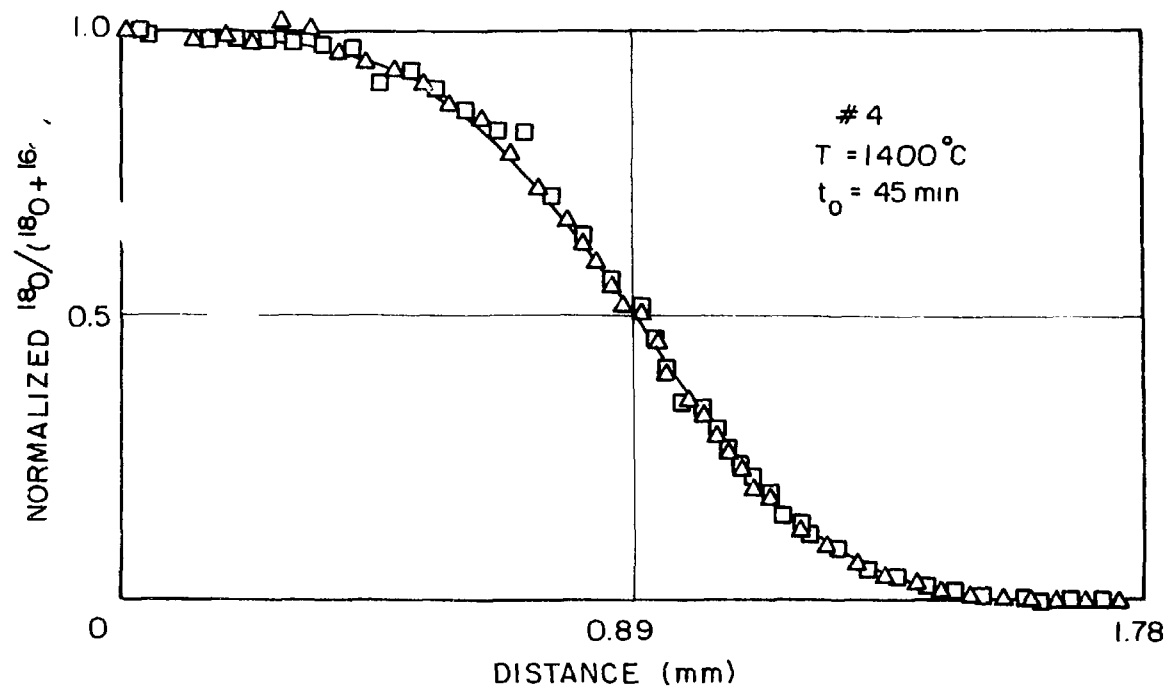
Figure 25.

XBL8010-6092
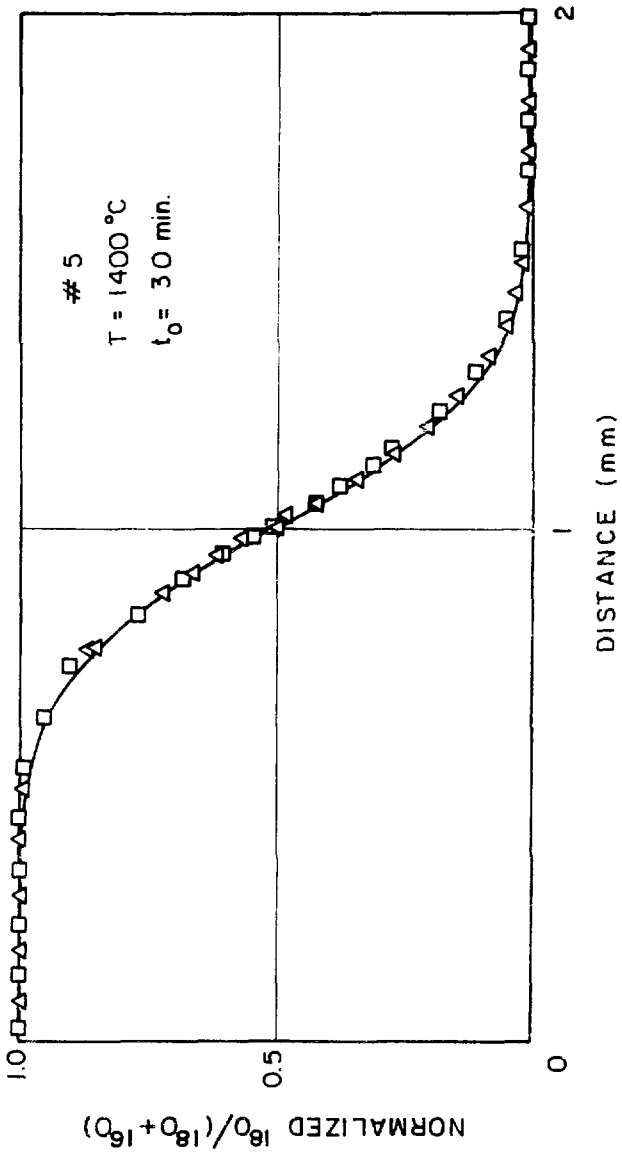
Figure 26.

XBL 8010-6123

Figure 27.

XBL 8010-6124

NORMALIZED $^{18}O/(^{18}O + ^{16}O)$

#5

T = 1400 °C

t_o = 30 min.

DISTANCE (mm)

XBL8010-6093
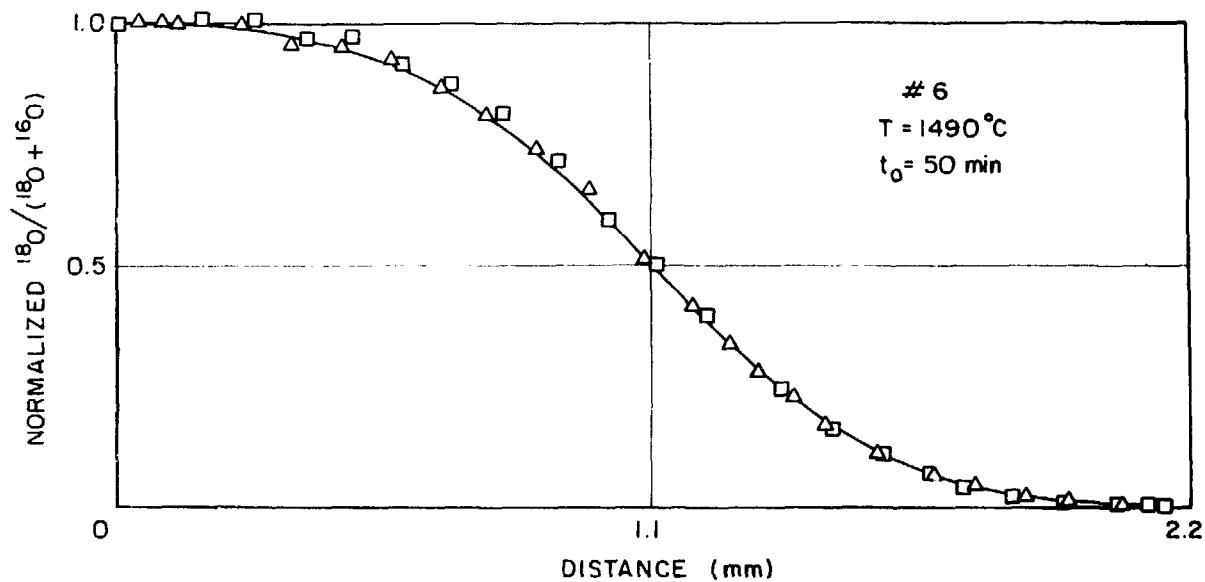
Figure 28.

Figure 29.

XBL 8010-6125
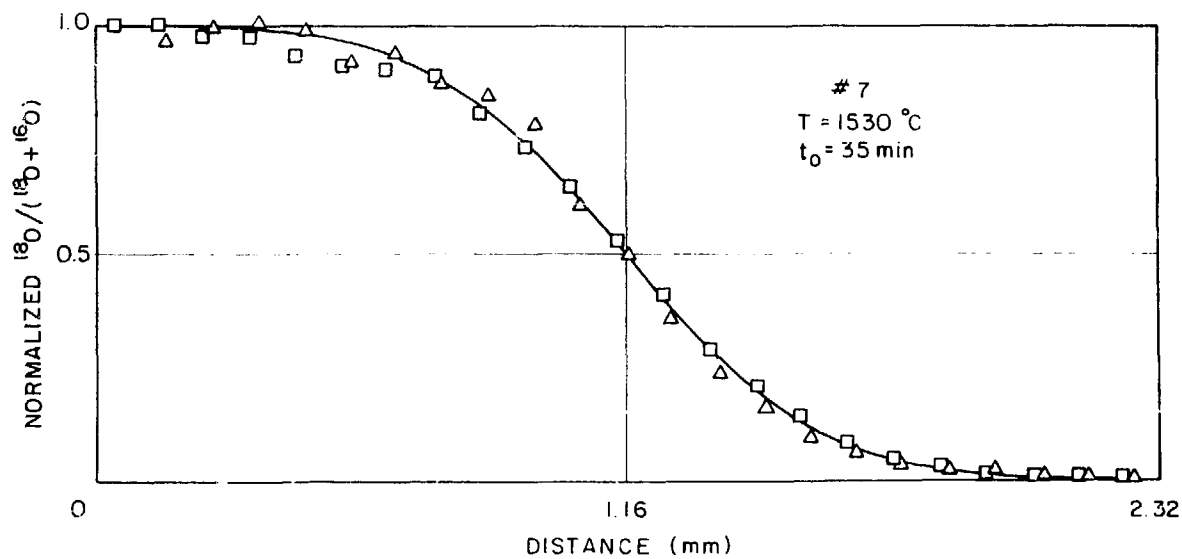
Figure 30.
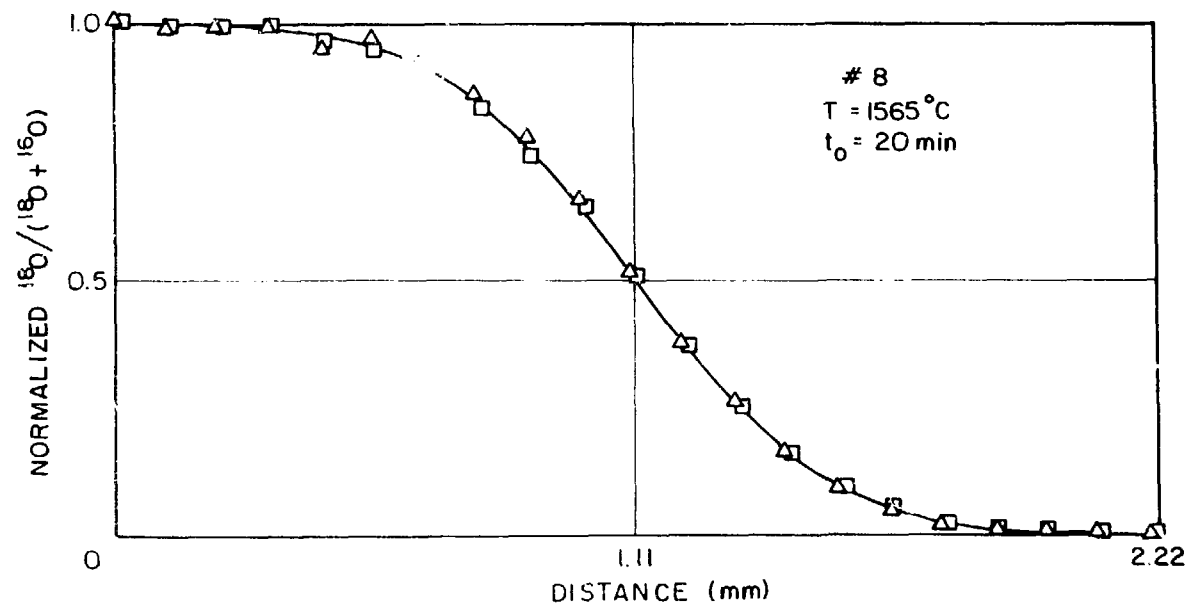
Figure 31.
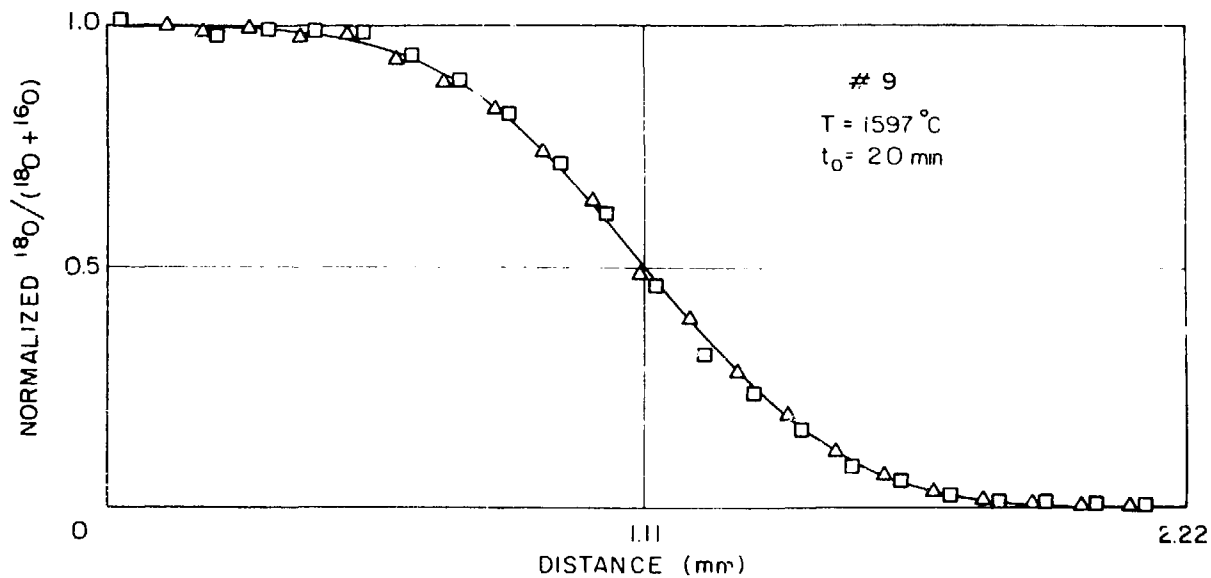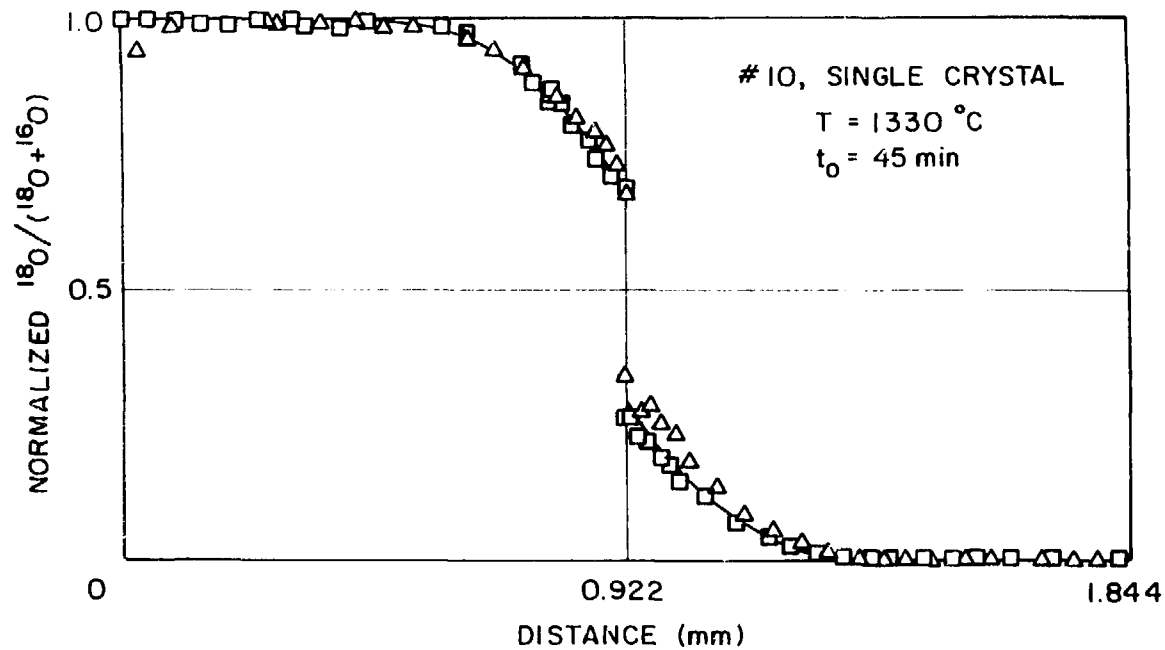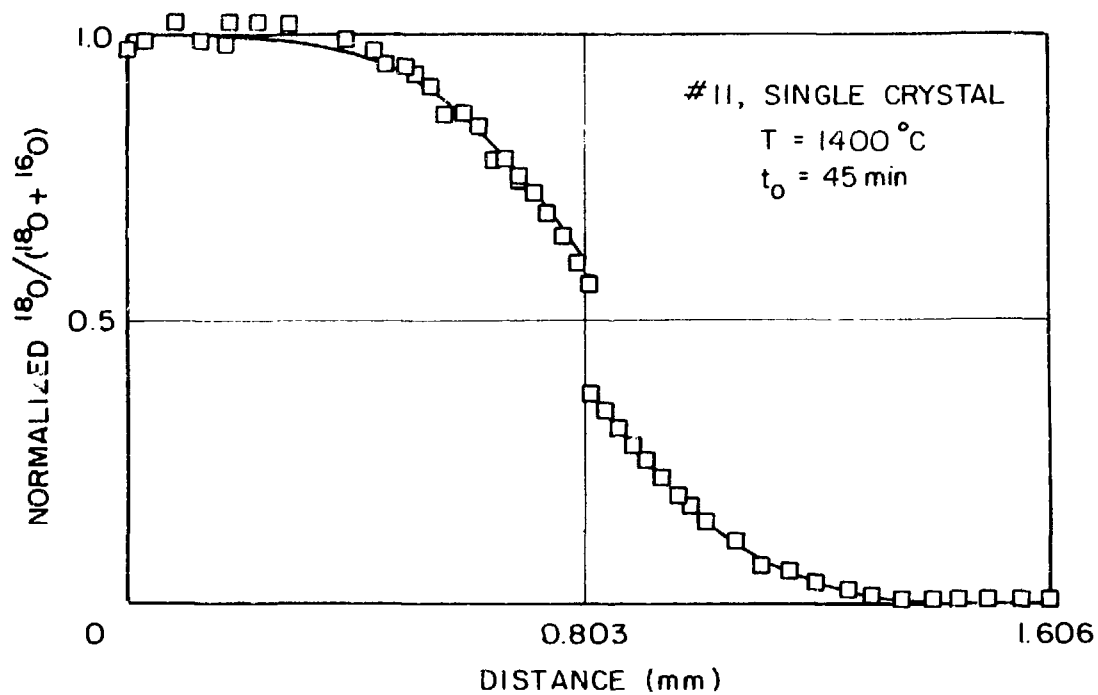
Figure 32.

XBL8010-6128

Figure 33.

XBL 8010-6129

Figure 34.

XBL 8010-6130

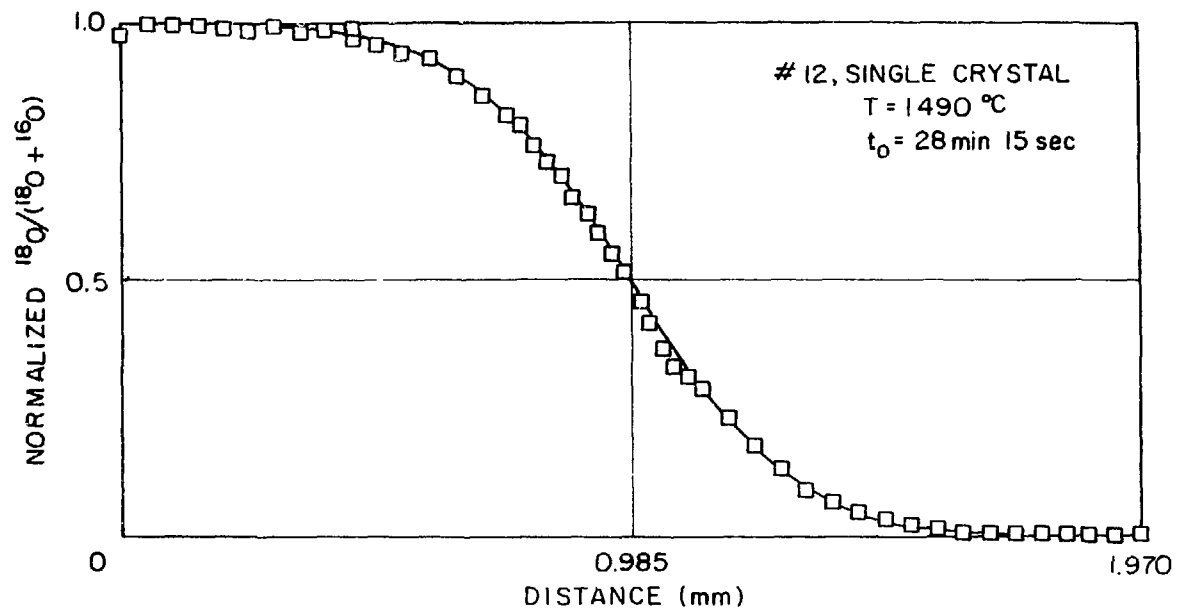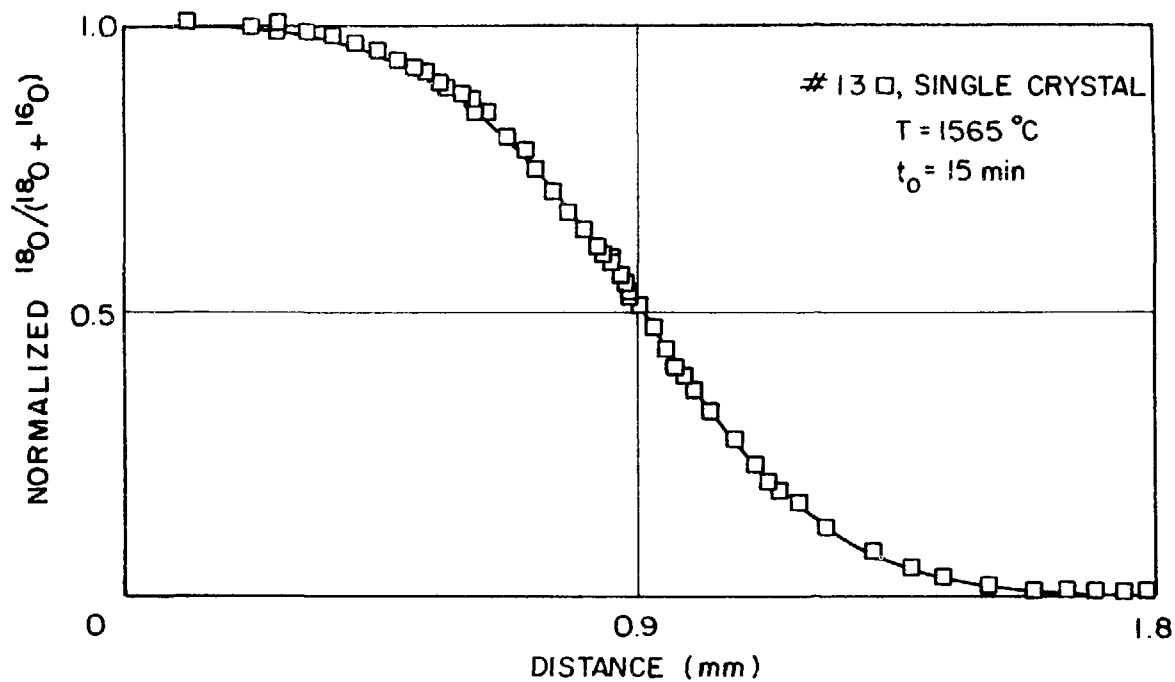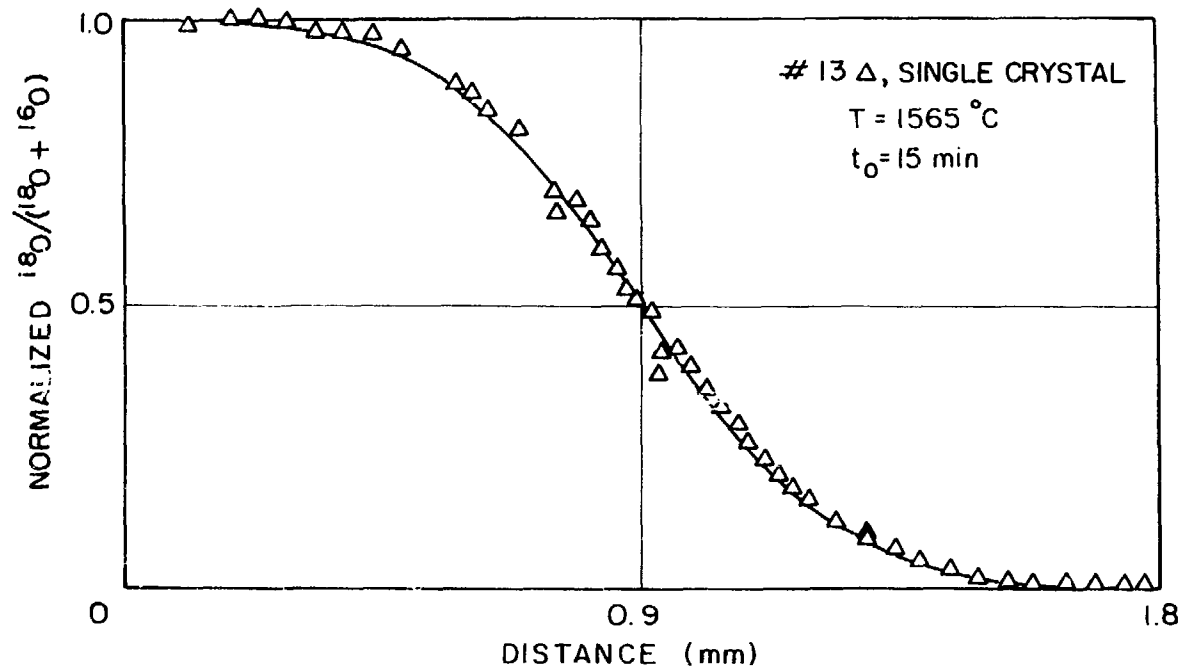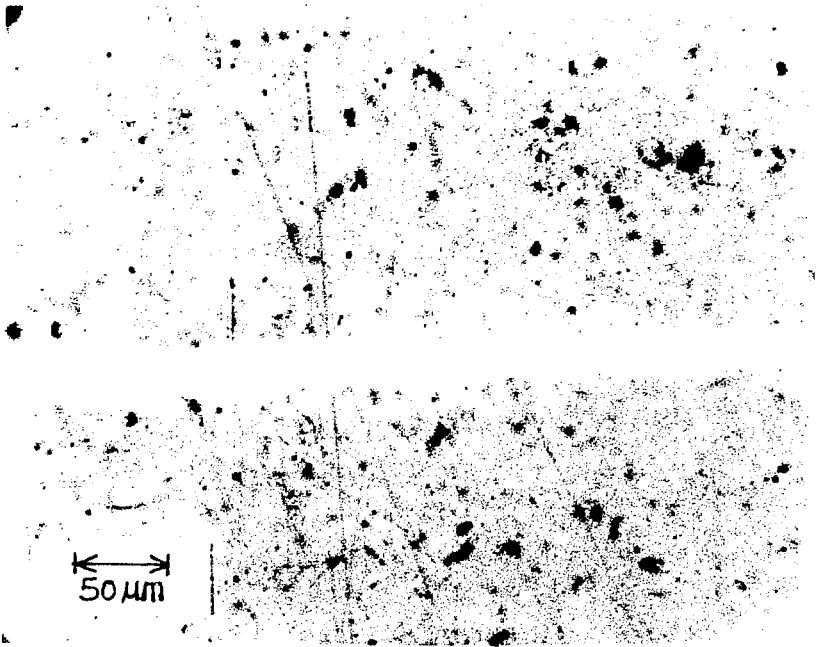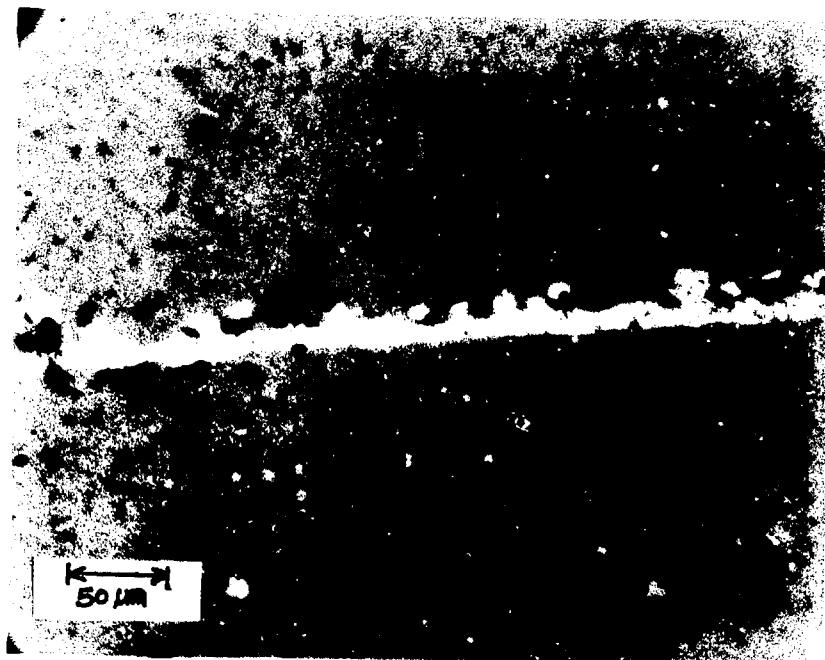Figure 35.

Figure 36.

XBL 8010-6132

Figure 37.

XBL 8010-6133

There were basically three different types of bonds observed between the two wafers.

(1) Continuous thick uranium layer (5~30 um) across the entire sample: As expected, samples of this type of bond yielded discrepancies in ^{18}O concentration across the interface. Samples No. 1, 2, 3, 10, 11 belong to this type. Shown in Fig. 38 are the photomicrographs of the interface of samples No. 2 and 11. The uranium layer is distinctly visible as a white band.

(2) Sintered interface: Naturally this type showed no ^{18}O discrepancies. Although two wafers were sintered together, the original interface was easily identifiable because a number of uranium particles remained along the interface (see Fig. 39). This type was observed in samples such as No. 8 and 12 which were annealed at high temperatures.

(3) Combination of (1) and (2): This type of specimen snowed some areas which were sintered and some which had a uranium layer (see Fig. 40). It is likely that this structure occurred because the wafers were not truly parallel and therefore the contact was not uniform. However, in every case of this type, the uranium layer was extremely thin (2-3 microns). For this type of samples one of the probe lines traversed the sintered area and the other crossed the uranium layer for the purpose of comparison. Those two profiles were always in good agreement and showed no

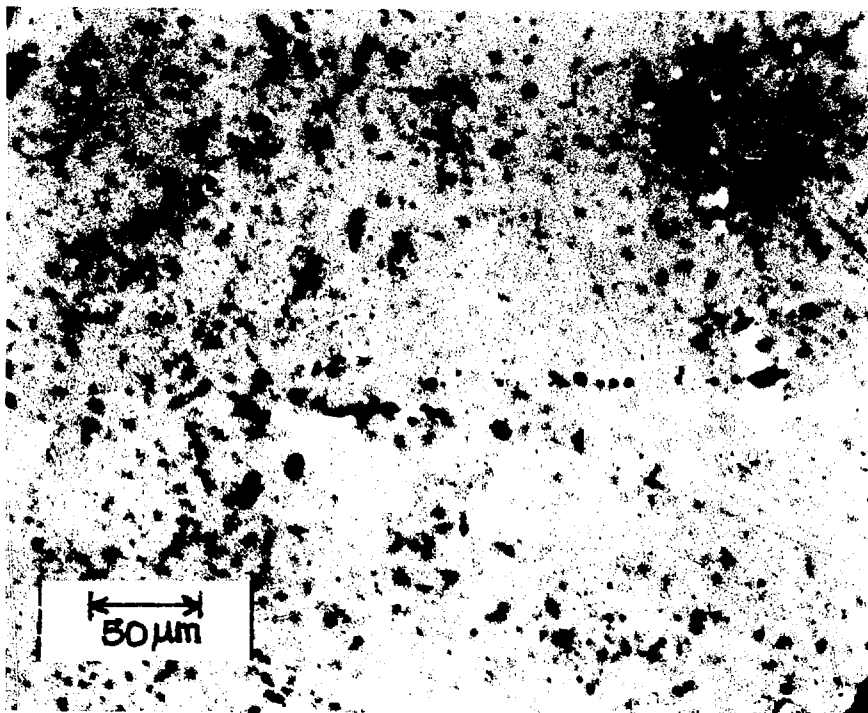XBB 800 11800

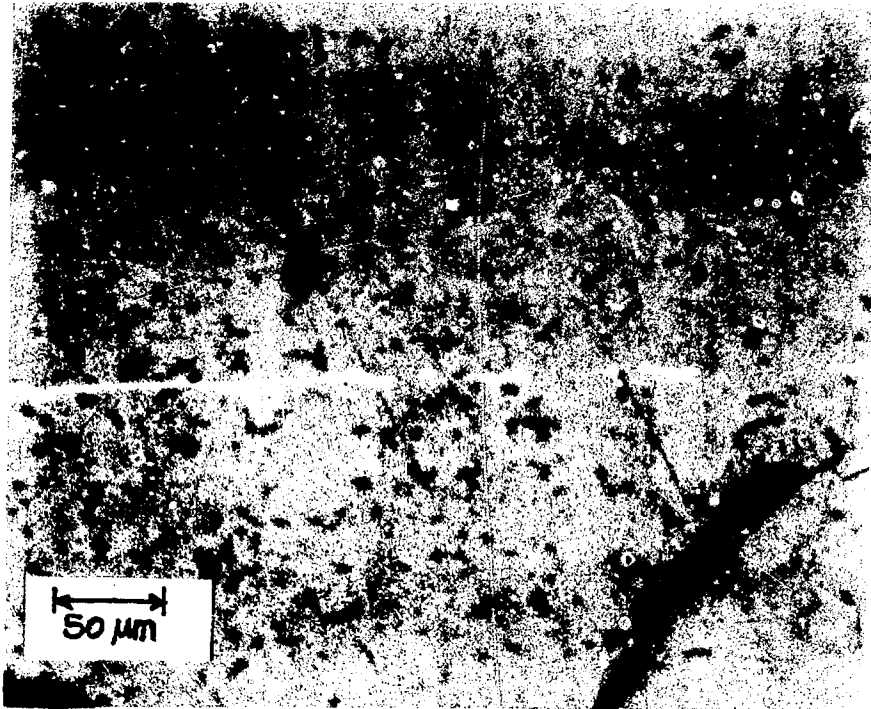Figure 38A. Thick uranium interface (sample #11).

88

XBB 800 11801

Figure 38B. Thick uranium interface (sample #2).

XBB 800 11798

Figure 39. Sintered interface (sample #8).

Figure 40. Half-sintered interface (sample #5).

significant discrepancies at the interface, most likely
because the uranium layer was extremely thin. Samples No. 4,
5, 6, 7, 9, 13 belong to this type.

In every sample, whenever the probe line crossed the uranium layer,
the ^{18}O concentrations of the points immediately adjacent to both
sides of the uranium layer were measured in order to detect any
discontinuity in ^{18}O concentration across the uranium layer.

The contact between liquid uranium and urania was excellent (see
Fig. 38a), which was essential to minimize the interfacial resistance.
No gap or voids were observed even when the surface was not smooth
(see Fig. 38b).

The normalized data were fitted to Eq. (13) using a computer code
MINUIT to find the best values of D and B. However, since time was
required to reach the operating temperature and to cool down after the
experiment, diffusion during these stages had to be taken into account.

Corrections were significant in higher temperature experiments
where the annealing time was relatively short and diffusion was fast.

As was indicated, the temperature could be raised slowly up to the
melting point of uranium without causing any premature diffusion. From
1100°C (near the melting point of uranium), the temperature was raised
rather rapidly up to the annealing temperature, which took at most
3 mins. Since this is a temperature range where urania is highly
plastic, this operation could be carried out rapidly without cracking
the samples.

The times required to heat the couple from 1100°C to the annealing
temperature, t_1, are shown in Table 10. Also shown are the cooling

times to $1100°C$ (t_2). Usually 2–3 mins. were taken for cooling from $1100°$ to $500°C$ so that even for the sintered diffusion couples it was assumed that below $1100°C$ diffusion annealing was negligible.

The nominal annealing times, t_0, are also tabulated.

To take these thermal transients into account, however, it is apparent from the nature of the problem that only an approximation is possible. Here, an effective t_{eff} was sought which would accommodate the diffusion anneal during these transient periods. Since the degree of diffusion anneal was a function of the product Dt, effort were concentrated on the value Dt itself to deduce the approximate value of t_{eff}.

The t_{eff} was defined as:

$$\int_0^{t_T} D \, dt = D_T \cdot t_{eff} \tag{28}$$

D_T is the diffusion coefficient at the annealing temperature and $t_T = t_1 + t_2 + t_0$, the total time for the experiment.

To calculate t_{eff}, $D(t)$ needs to be known. Therefore, t_{eff} and D should be obtained by an iterative process.

It was assumed that the temperature T' changed linearly with time:

$$T' = 1373 + (T-1373)(t/t_i) , \quad 0 \le t \le t_1$$

$$T' = T - (T-1373) \left(\frac{t-t_1-t_0}{t_2}\right), \quad t_1+t_0 \le t < t_1+t_2+t_0 \tag{29}$$

and T is the annealing temperature in $°K$.

As temperature changes, the corresponding stoichiometry of the two phase boundary also changes. In near-stoichiometric material, the following equation can be assumed for oxygen self-diffusion by the vacancy mechanism [49].

$$D = D_0^V \theta_V (1-\theta_V) \exp(-\Delta H_V / RT) \tag{30}$$

θ_V is vacancy concentration ($x/2$ in UO_{2-x}), ΔH_V is the activation energy of vacancy migration, and D_0^V is a constant. The equation will be discussed in greater detail in the next chapter.

The iteration was started by fitting Eq. (13) to the normalized data using $t=t_0$, the nominal annealing time. Fitting yielded diffusion coefficients for each experiment. This first diffusion coefficient obtained is shown in Table 11 as $D_{(1)}$. The D_0^V and ΔH_V of Eq. (30) were calculated by plotting $\ln[D_{(1)}/ \theta_V(1-\theta_V)]$ vs $1/T$ using linear fitting.

From Eq. (27) and (30),

$$D_{(1)} = 0.5 D_0^V \exp(3.678 - 12675/T')$$
$$\left\{ 1 - 0.5 \exp(3.678 - 12675/T') \right\} \exp(-\Delta H_V / RT') \tag{31}$$

Combining Eqs. (31) and (29), $D_{(1)}(t)$ was obtained and from Eq. (28) t_{eff} was determined. The integration was done graphically. The first t_{eff} values are shown in Table 11 as t'_{eff}. Using t'_{eff}, new diffusion coefficients were obtained ($D_{(2)}$ in the table) and second iteration started. After the third iteration it was apparent

Table 11. Effective times and diffusion coefficients during the iteration and the final D values and effective times.

RUN	T°C	t_o mins	$D_{(1)} \times 10^7$ cm²/sec	t'_{eff}	$D_{(2)} \times 10$ cm²/sec	t_{eff}	$D \times 10^7$ cm²/sec
1	1190	340	0.25	341	0.249	341	0.249
2	1257	180	0.47	181	0.467	181	0.466
3	1330	20	0.86	20.8	0.828	20.8	0.823
4	1400	45	1.45	46.8	1.398	46.6	1.400
5	1400	30	1.43	31.8	1.352	31.6	1.357
6	1490	50	2.43	52.1	2.237	51.8	2.346
7	1530	35	.65	36.5	2.536	36.4	2.551
8	1565	20	3.58	21.8	3.278	21.6	3.279
9	1597	20	4.48	21.9	4.087	21.7	4.129
10	1330	45	0.85	46.4	0.820	46.4	0.820
11	1400	45	1.11	46.8	1.072	46.6	1.072
12	1490	28	1.93	30.4	1.791	30.3	1.799
13	1565	15	4.19	16.8	3.741	16.6	3.786

that values had converged adequately to the t_{eff} and D figures shown
in the table.

Values of D were used to deduce D_0^V and ΔH_V of Eq. (30). In
Figs. 41 and 42, $\ln[D/\theta_V(1-\theta_V)]$ vs $1/T$ is plotted for the poly-
crystalline samples and single crystal samples, respectively. Linear
least squares fitting yielded $D_0^V = 4.4 \times 10^{-4}$ and $\Delta H_V = 11.7 \pm 3.0$ kcal/
mole for polycrystalline samples;

$$D = 4.4 \times 10^{-4} \theta_V(1-\theta_V) \exp(-11700/RT) \tag{32}$$

Similarly, for single crystals $D_0^V = 5.9 \times 10^{-4}$ and $\Delta H_V = 13.0 \pm 10.2$ kcal/
mole were obtained;

$$D = 5.9 \times 10^{-4} \theta_V(1-\theta_V) \exp(-13000/RT) \tag{33}$$

It should be noted that two separate experiments (No. 4 and No. 5
in Table 11) were conducted at 1400°C for different annealing time; one
for 30 mins. and the other for 45 mins. This was to check the
reproducibility. As can be seen in Table 11, the values of D obtained
are very close to each other.

In order to clearly demonstrate the difference between single
crystal and polycrystalline samples, one of the 1400°C polycrystalline
experiments (No. 4) and single crystal experiment No. 11 were conducted
simultaneously. This was achieved by simply stacking the single
crystal diffusion couple on top of the polycrystalline couple in a
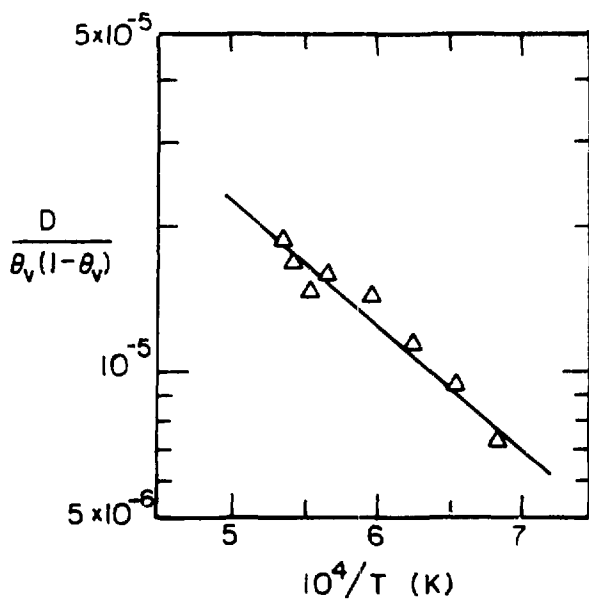
XBL 8010-6088

Figure 41.   Plot of polycrystalline data to determine D_0^V and ΔH_V.
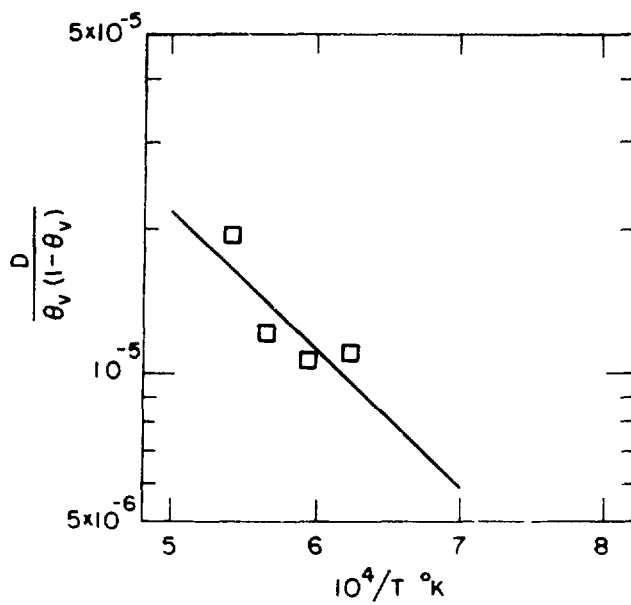
XBL8010-6101

Figure 42. Plot of single crystal data to determine D_0^v and ΔH_v.

crucible deeper than ordinary ones (see Fig. 43). A 0.005 in. thick

rhenium foil was used to separate the two couples. By this arrange-

ment, identical temperature history and all other conditions could be

imposed to the two couples. The results show clearly that diffusion

is slower in the single crystal (see No. 4 and No. 11 in Table 11).

The difference is not very large because of the unusually large grain

size (~200 μm) of the polycrystalline samples.

Since the single crystal correlation has fewer data points and is

not as good as the polycrystalline correlation, only Eq. (32) will be

used in subsequent analysis.
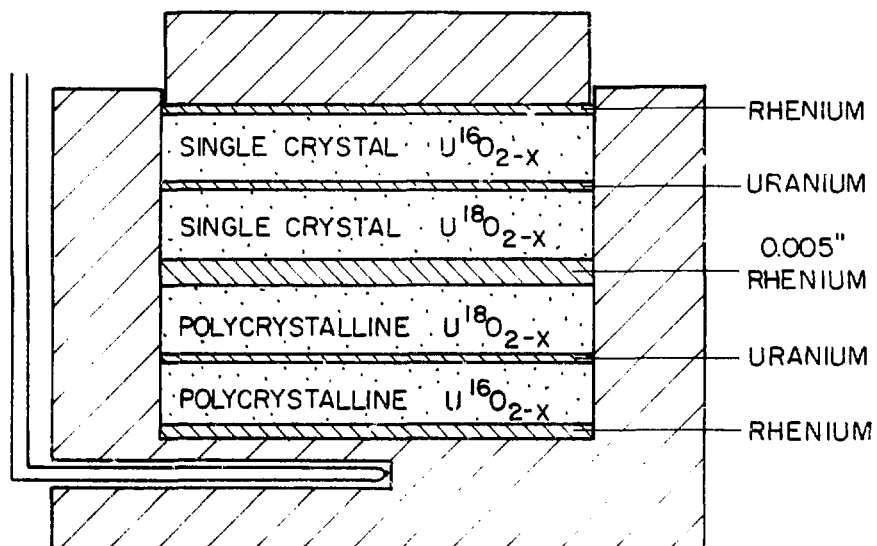
XBL 8010-6102

Figure 43.   Double diffusion couple arrangement.

5. DISCUSSION

5.1 Comparison with Other Materials of Fluorite Structure

Due to the similarity in their crystal structure it has been widely believed that UO_{2-x} has the same type of crystal defect (anion vacancy) and diffusion mechanism (vacancy) as CeO_{2-x} and PuO_{2-x}. However, this supposition has never been confirmed experimentally. On the contrary, thermodynamic studies favor the excess uranium model [39].

Since the stoichiometry and temperature were changed simultaneously in the present experiment, it is difficult to separate the stoichiometry contribution to the enhanced diffusion at higher temperature. However, comparing the present data for UO_{2-x} with existing data of stoichiometric UO_2 [1] at the same temperature, it is readily seen that the present data are almost two orders of magnitude higher than those of stoichiometric UO_2. This effect can only be attributed to non-stoichiometry, thereby demonstrating the existence of defects in the anion sublattice, i.e., oxygen vacancies in UO_{2-x}. Based on this fact the diffusion coefficient is analyzed in terms of vacancy contribution and migration energy.

It is well known from the random walk theory that for a vacancy mechanism the diffusion coefficient can be expressed as [49]:

$$D_v = D_0^v \theta_v \ (1-\theta_v) \ exp(-\Delta H_v/RT) \qquad (35)$$

where D_0^v is the pre-exponential factor, ΔH_v is the vacancy migration energy, θ_v is vacancy concentration, and $(1-\theta_v)$ is diffusion path probability.

In substantially hypostoichiometric UO_{2-x}, the concentration of oxygen interstitials is negligible compared to vacancies, and therefore interstitial contribution to diffusion is also negligible. In addition, thermally generated vacancies are negligible. The analysis of the diffusion data in the previous chapter to yield Eqs. (32) and (33) was based on these two assumptions.

Experimental results on CeO_{2-x} and PuO_{2-x} are compared with the present work at different stoichiometries in Table 12. For the present work the result of polycrystalline samples were used. It is seen that both the activation energies and pre-exponential factors are in excellent agreement with those of CeO_{2-x} and PuO_{2-x}.

The current model is based on random walk theory with no interactions among defects, which is valid only for small nonstoichiometries. Therefore, the disagreement in Table 12 between $CeO_{1.80}$ and the remaining values is attributed to the large deviation in the stoichiometry of the former and therefore should be explained in terms of defect clustering or microdomains of ordered regions [12].

5.2   Oxygen Diffusion in Near-Stoichiometric $UO_{2\pm x}$

5.2.1   Introduction

As indicated earlier, there have been several studies [1,2,4,7] of oxygen diffusion in stoichiometric UO_2 and they are in reasonably good agreement. The diffusion mechanism, however, is not very well established primarily due to the lack of experimental data on vacancy migration.

Table 12. Comparison of oxygen diffusion in UO_{2-x} with CeO_{2-x} and PuO_{2-x}.

X	CeO_{2-x}[12,13]	PuO_{2-x}[15]	UO_{2-x}
0.005		$0.2 \times 10^{-5} \exp(-10900/RT)$	$0.11 \times 10^{-5} \exp(-11700/RT)$
0.01		$0.5 \times 10^{-5} \exp(-11100/RT)$	$0.22 \times 10^{-5} \exp(-11700/RT)$
0.03		$1.3 \times 10^{-5} \exp(-11300/RT)$	$0.65 \times 10^{-5} \exp(-11700/RT)$
0.05		$1.6 \times 10^{-5} \exp(-10800/RT)$	$1.07 \times 10^{-5} \exp(-11700/RT)$
0.08	$1.51 \times 10^{-5} \exp(-11900/RT)$		$1.68 \times 10^{-5} \exp(-11700/RT)$
0.2	$6.16 \times 10^{-6} \exp(-3600/RT)$		

In their early study Auskern et al. [2] simply assumed the applicability of the interstitialcy mechanism to stoichiometric UO_2 as well as to hyperstoichiometric UO_{2+x} and calculated the energy to form Frenkel defects to be 70 kcal/mole, which was later supported by the heat capacity measurement of Szwarc [40]. More recently, Breitung [8] and Murch et al. [9] attempted to include both interstitial and vacancy contributions in the diffusion model. However, due to different estimates of the vacancy migration energy, their results were quite different, supporting interstitialcy and vacancy mechanisms, respectively. By theoretical calculation, Catlow et al. [16] obtained 5.8 kcal/mole for the energy of vacancy migration. Also calculated was a Frenkel energy of 11.5 kcal/mole. Assuming a vacancy mechanism in stoichiometric UO_2 instead of an interstitialcy mechanism, these two theoretical values yielded a diffusion activation energy of 65.6 kcal/ mole, which was in good agreement with the experimental result.

As can be seen, the disagreements arise from lack of reliable data on vacancy migration energy coupled with uncertainty in Frenkel energy.

Since experimental results in UO_{2-x} are now available from the present work, it should be useful to look into this problem in detail.

5.2.2 Diffusion Model

Throughout the work it is assumed that the dominant defect in $UO_{2\pm x}$ is the anion Frenkel defect; Schottky defects are neglected. The defect model is based on the following relations:

(1) Defect formation:

$$0_0 + V_i \overset{\rightarrow}{\underset{\leftarrow}{}} V_0 + 0_i \tag{36}$$

$$K_F = \frac{\theta_v}{1-\theta_v} \quad \frac{\theta_i}{1-\theta_i} = \exp(\Delta S_F/R)\exp(-\Delta H_F/RT) \tag{37}$$

where 0_0 = oxygen ion in regular lattice site

V_i = unoccupied interstitial site

0_i = oxygen in interstitial site

V_0 = vacancy in regular lattice site

$$\theta_v = \frac{\text{number of anion vacancies}}{\text{number of anion lattice sites}} = \frac{N_v}{N_0} = \frac{N_v}{2N_U} \tag{38}$$

$$\theta_i = \frac{\text{number of interstitials}}{\text{number of interstitial sites}} = \frac{N_i}{\alpha N_U} \tag{39}$$

N_v = number of anion vacancies/cc

N_U = number of cation sites/cc

N_0 = number of anion sites/cc

ΔS_F = entropy of Frenkel defect formation

ΔH_F = entropy of Frenkel defect formation.

The number of available anion interstitial sites of UO_2 and UO_{2-x} is equal to number of uranium atoms. In UO_{2+x}, however, as the number of interstitials increases, occupiable interstitial sites gradually become selective. α is the parameter that accommodates this effect in UO_{2+x}, for which Contamin et al. [3] developed the semi-empirical expression;

$$\alpha = \frac{2}{(2+x)(1+10^3x^3)^{1/2}} \tag{40}$$

For UO_2 and UO_{2-x}, $\alpha=1$.

(2) Electroneutrality:

$$x = \alpha\theta_i - 2\theta_v \tag{41}$$

Solving Eqs. (37) and (41) for θ_i and θ_v,

$$\theta_i = \frac{-B + (B^2 - 4AC)^{1/2}}{2A} \tag{42}$$

and

$$\theta_v = \frac{1}{2}(\alpha\theta_i - x) \tag{43}$$

where

$$A = \frac{\alpha}{2}(1-K_F)$$

$$B = K_F(1 + \frac{\alpha}{2} + \frac{x}{2}) - \frac{x}{2} \tag{44}$$

$$C = -K_F(1 + \frac{x}{2})$$

Assuming that in $UO_{2\pm x}$ (i) oxygen diffusion can proceed by both vacancy and interstitial migration simultaneously, and (ii) the movements of these two species are independent of each other, the total oxygen diffusion coefficient can be expressed as the sum of the two terms:

$$D = D_{(v)} + D_{(i)} \qquad (45)$$

In substantially hypostoichiometric UO_{2-x}, $D_{(i)} \approx 0$. Thus, from Eq. (35)

$$D = D_{(v)} = D_0^v \theta_v (1-\theta_v) \exp(-\Delta H_v/RT) \qquad (46)$$

Similarly, in substantially hyperstoichiometric UO_{2+x}, $D_{(v)} \approx 0$, and

$$D = D_{(i)} = D_0^i \theta_i (1-\theta_i) \exp(-\Delta H_i/RT) \qquad (47)$$

From the present experiment, $D_0^v = 4.4 \times 10^{-4}$ and $\Delta H_v = 11.7$ kcal/mole were obtained. D_0^i and ΔH_i were obtained by re-analyzing the existing oxygen diffusion data of UO_{2+x}. Only the data of Contamin et al. [3] and Murch [6] were used because their experimental methods were considered to be most accurate.

In substantially hyperstoichiometric UO_{2+x}, the thermally generated interstitials are negligible. Thus, from Eq. (43), $\theta_i \approx \frac{x}{\alpha}$. In Fig. 14, $\ln[D_{(i)}/\theta_i(1-\theta_i)]$ is plotted vs. $1/T$. Least squares fitting yielded $D_0^i = 4.7 \times 10^{-3}$ and $\Delta H_i = 21.8 \pm 13.0$ kcal/mole. Thus,

$$D_{(i)} = 4.7 \times 10^{-3} \theta_i (1-\theta_i) \exp(-21800/RT) \qquad (48)$$

Combining Eqs. (32), (48), and (45),
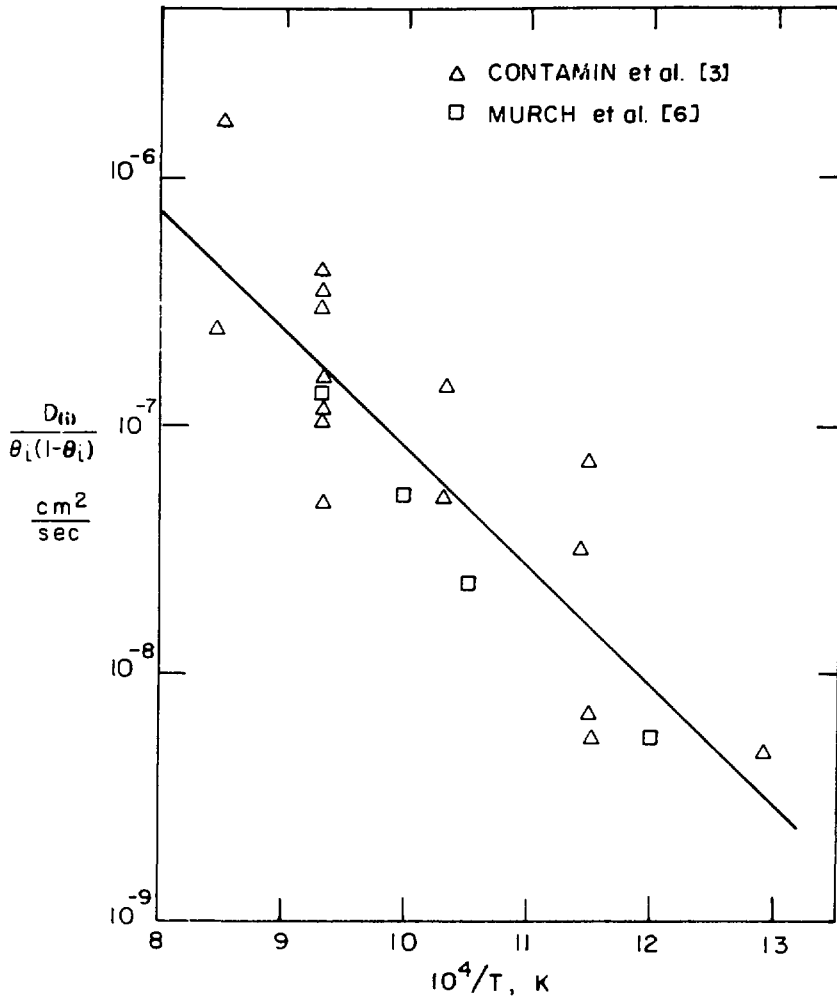
Figure 44. Re-analysis of the diffusion data of UO_{2+x}.

XBL 8011-6351

$$D = 4.4 \times 10^{-4} \theta_v (1-\theta_v) \exp(-11700/RT) + 4.7 \times 10^{-3} \theta_i (1-\theta_i) \exp(-21800/RT)$$

$$(49)$$

Using the computed code MINUIT, data for stoichiometric UO_2 were fitted to Eq. (49) combined with Eqs. (42) and (43) with $\alpha=1$ and $x=0$ to obtain the Frenkel energy and entropy. Only the data of Marin et al. [1] were used; Data of Auskern et al. [2] and Roberts et al. [7] were excluded because of their unusually large pre-exponential factor which probably resulted from other rate controlling processes affecting the gas-solid isotopic exchange method [1,6]. Also, the stoichio-metries of their samples were not as close to 2.0 as those of Marin et al. [1].

Figure 45 shows the data points of Marin et al. [1] and the fitted curve (solid line) for $\Delta H_F = 85.6 \pm 9.2$ kcal/mole and $\Delta S_F = 18.2 \pm 7.2$ e.u. These may be compared with Szwarc's calculation of $\Delta H_F = 71.3 \pm 2.2$ kcal/mole and $\Delta S_F = 14.8 \pm 0.84$ e.u. [40].

Also shown in Fig. 45 are the contribution of interstitials and vacancies, $D_{(i)}$ and $D_{(v)}$. At very low temperatures, vacancies are the primary species that contributes to the total diffusion in UO_2. In the temperature range of 300–1800°C, however, neither of the species is completely predominant; and at 1400°C the contributions of the two species are approximately equal. Above this temperature $D_{(i)} > D_{(v)}$, and below this temperature $D_{(i)} < D_{(v)}$. The fractional contributions of the two species are depicted in the upper portion of Fig. 45.

Since one of the two terms in Eq. (49) becomes negligible in a substantially nonstoichiometric region, this equation provides a
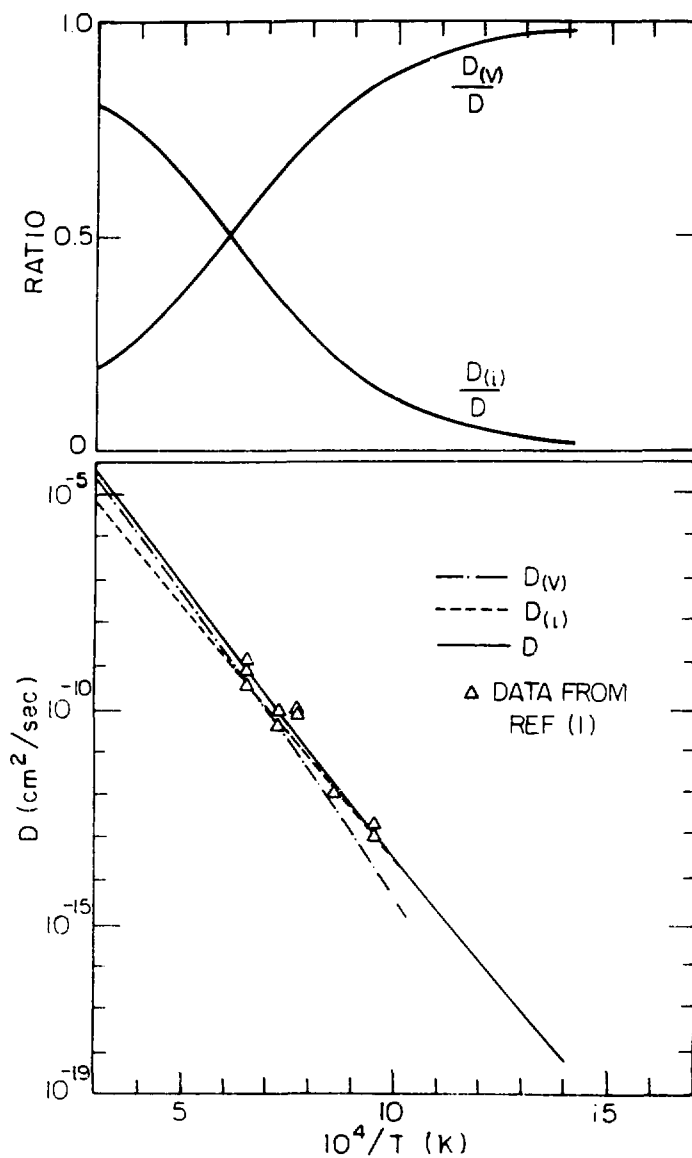
XBL8010-6089

Figure 45. Fitted curve to the diffusion data of stoichiometric
UO₂ using optimum values of Frenkel energy and entropy.
Absolute and fractional contributions of interstatials
and vacancies are also plotted.

unified diffusion model in $UO_{2\pm x}$ for all stoichiometries. However, it should be emphasized that the current model is valid only when the point defects are independent of each other.

Using Eq. (49), diffusion coefficients in near-stoichiometric UO_{2-x} and UO_{2+x} were calculated and the results are shown in Fig. 46 and Fig. 47, respectively.

Compared to Fig. 46, Murch et al. [9] predict 2-3 orders of magnitude higher values of D in UO_{2-x}, due to the low ΔH_v and high pre-exponential factor they employed.

5.3 Excess Enthalpy and Frenkel Energy of UO_2

It is well known that the specific heat and the enthalpy of UO_2 display unusually rapid increase from $1500°K$ to $3100°K$ [41-44], which cannot be explained by lattice vibrations. Szwarc [40] attributed all of this excess enthalpy to Frenkel disorder to deduce the Frenkel energy and entropy. Supporting this interpretation was the oxygen diffusion data in stoichiometric UO_2 with the assumption of an interstitialcy mechanism [2]. However, in light of the present work, the diffusion model should be altered, thereby undermining Szwarc's interpreation of the excess enthalpy.

Recently, a series of attempts were made to re-interpret the excess enthalpy in terms of electronic excitation [46-48]. Although quantitative results could not be obtained because the electronic structure of UO_2 is not well established, it was demonstrated that the electronic contribution to the enthalpy could be significant.

In the previous section, the Frenkel energy of $\Delta H_F = 85.6$ kcal/mole and entropy of $\Delta S_F = 18.2$ e.u. were obtained by fitting
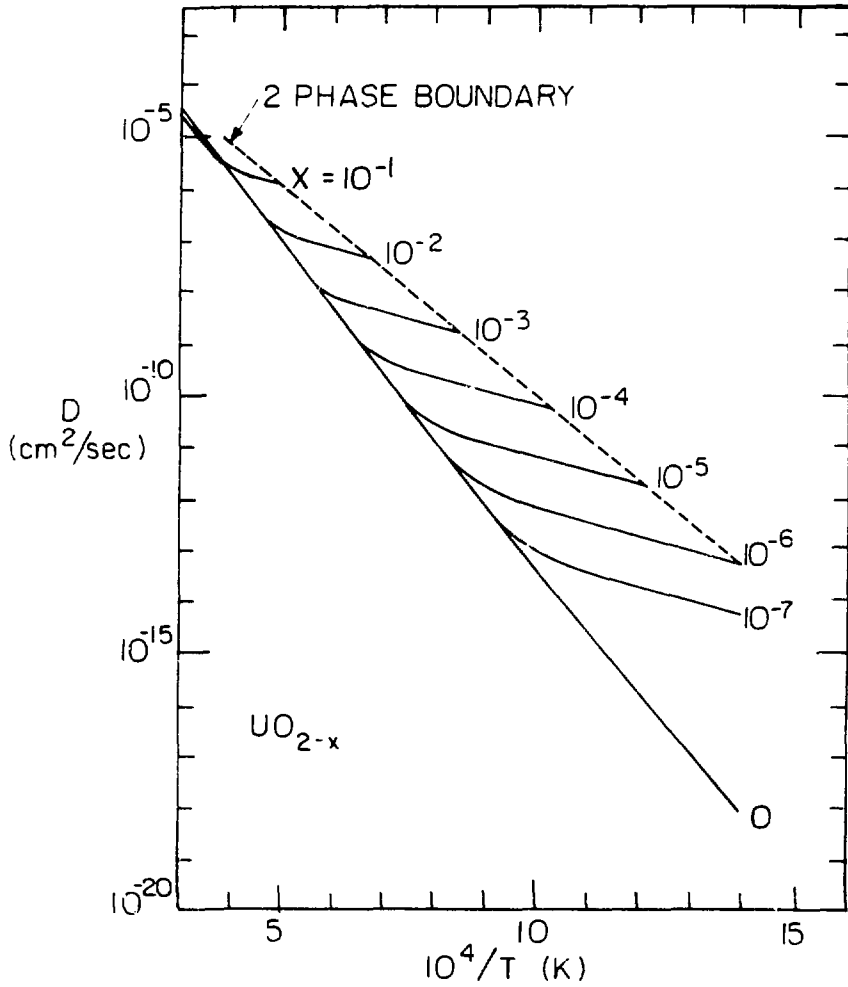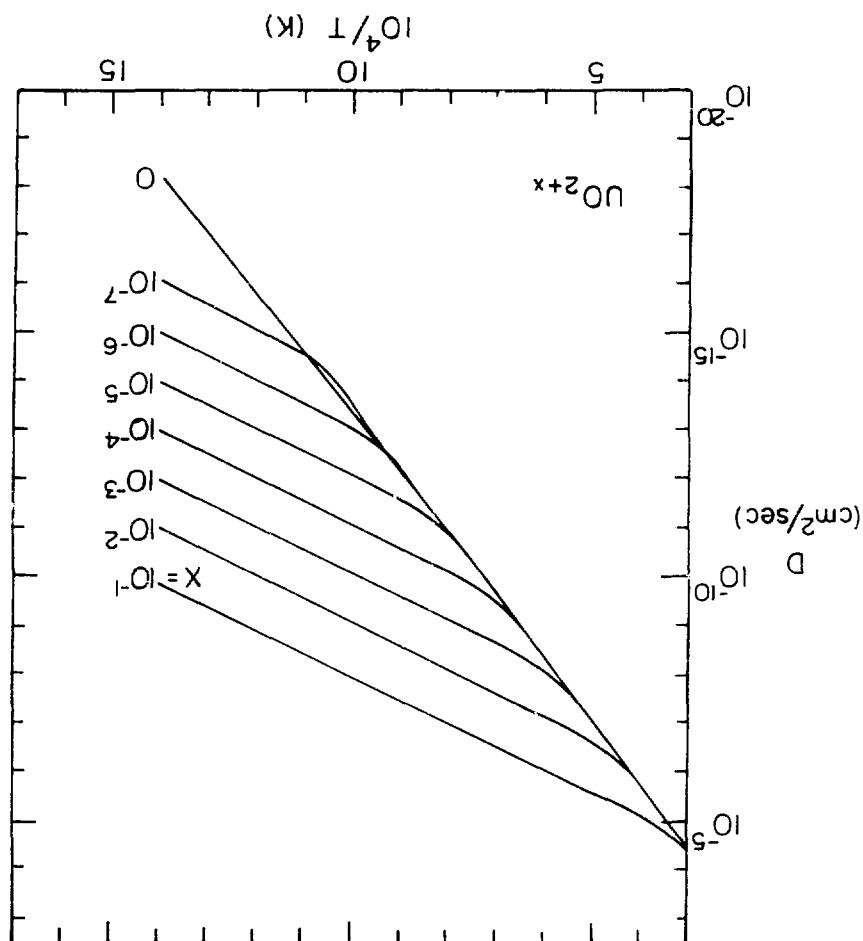
Figure 46. Predicted oxygen diffusion coefficients in UO_{2-x}.

Figure 47. Predicted oxygen diffusion coefficient in UO_{2+x}.

XBL8010-6090

the oxygen diffusion data of stoichiometric UO_2 to the present model. This Frenkel energy is higher than Szwarc's calculation of 71.3 kcal/mole [40]. This means that the population of Frenkel defects is less than predicted by Szwarc's model and therefore their contribution to the excess enthalpy is also smaller.

Her   ... the rest of the excess enthalpy is ... ...ed to arise from the electronic contribution. Therefore, the observed enthalpy, ΔH, of UO_2 can be written as:

$$\Delta H = \Delta H_{ph} + \Delta H_{Fr} + \Delta H_{el} \qquad (50)$$

where ΔH_{ph}, ΔH_{Fr}, ΔH_{el} are enthalpy due to the lattice vibration, Frenkel disorder, and electronic exciation, respectively.

Collecting data from various studies, Kerrisk et al. [44] developed equations for enthalpy and heat capacity of UO_2 that represent the data. Although they also attributed all of the excess enthalpy to Frenkel disorder, the phonon terms in their equations still represent the low temperature data very well:

$$\Delta H_{ph} = K_1 \theta \left\{ [\exp(\theta/T)-1]^{-1} - [\exp(\theta/293)-1]^{-1} \right\} +$$
$$K_2(T^2 - 293^2) \qquad (51)$$

where $K_1 = 19.1450$ cal/mole-°K

$K_2 = 7.84733 \times 10^{-4}$ cal/mole-°K

$\theta = 535.285$°K .

The Frenkel disorder term can be derived as [40]:

$$\Delta H_{Fr} = \sqrt{2} \quad \Delta H_F exp(\frac{\Delta S_F}{2R}) \quad exp(-\frac{\Delta H_F}{2RT}) \tag{52}$$

where $\Delta H_F = 85.6$ kcal/mole

$\Delta S_F = 18.2$ e.u.

MacInnes [46] calculated the electronic contribution by introducing two models using two-band structure; valence band and conduction band, with a band gap of E_g. Using standard technique of the semiconductor theory, the energy absorbed by the band structure per unit volume at a given temperature was obtained as:

$$E = \frac{1}{2\pi^2} \left(\frac{2m^*}{h^2}\right)^{3/2} \left(\frac{N_d}{n_0}\right)^{1/2} \left[(\frac{3}{2}) \quad (kT)^{5/2} + \right.$$

$$\left. E_g(\frac{1}{2})! (kT)^{3/2}\right] \exp(-E_g/2kT) \tag{53}$$

N_d = number of electrons per unit volume in the valence band

$n_0 = 2(2\pi m^* kT/h^2)^{3/2}$

h = Planck's constant

$h = h/2\pi$

m^* = electronic effective mass

m_e = electron mass.

Following Catlow [45], MacInnes assumed that the valence band was comprised of 4f orbitals, and accordingly assigned 14 electrons to it. However, as Thorn et al. [47] indicated, to use 5f orbitals as the valence band may be more plausible than 4f. Thorn et al. [47] found

that two electrons could be assigned to the 5f orbitals. Using 5f orbitals for valence band in Eq. (53), ΔH_{el}(cal/mole) can be written as:

$$\Delta H_{el} = (\frac{m^*}{m_e})^{3/4} [1.789 \times 10^{-3} T^{7/4} +$$

$$6.003 \times 10^{-4} \Delta E \cdot T^{3/4}] \exp(-\Delta E/2RT) \tag{54}$$

ΔE is the electronic activation energy in cal/mole.

The reported enthalpy data [42,43] were fitted to Eq. (50) using Eqs. (51), (52), and (54) to obtain the optimum values of (m^*/m_e) and ΔE. In Fig. 48, the fitted ΔH curve and the data points are shown. Also shown are ΔH_{ph}, and the excess enthalpy ΔH_{ex} ($=\Delta H-\Delta H_{ph}$). Fitting yielded $(m^*/m_e) = 7.6\pm0.1$ and $\Delta E = 45.0\pm0.3$ kcal/mole, respectively. The ΔE value obtained is equivalent to a band gap of 2.0 ev, which is in good agreement with the reported values: 1.8~2.3 ev obtained from electrical conductivity data between 1400°K and 3000°K [52] and 2.1 ev obtained from reflectivity data [53].

Electronic contribution ΔH_{el} and Frenkel contribution ΔH_{Fr} are calculated seperately and shown in Fig. 49. Also shown on the same temperature scale are the fractional contributions of the two effects; $\Delta H_{el}/\Delta H_{ex}$ and $\Delta H_{Fr}/\Delta H_{ex}$. As temperature increases the fraction of electronic excitation decreases; at 3000°K it accounts for approximately 13 percent of the total excess enthalpy.
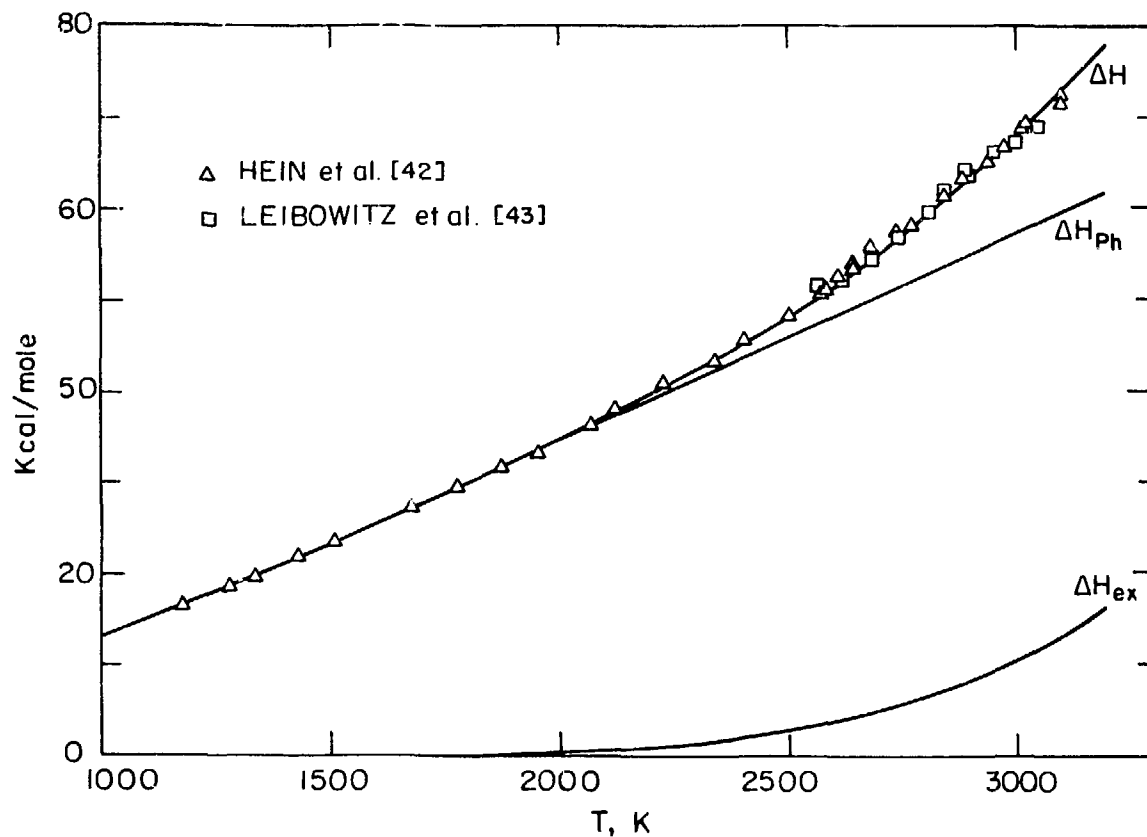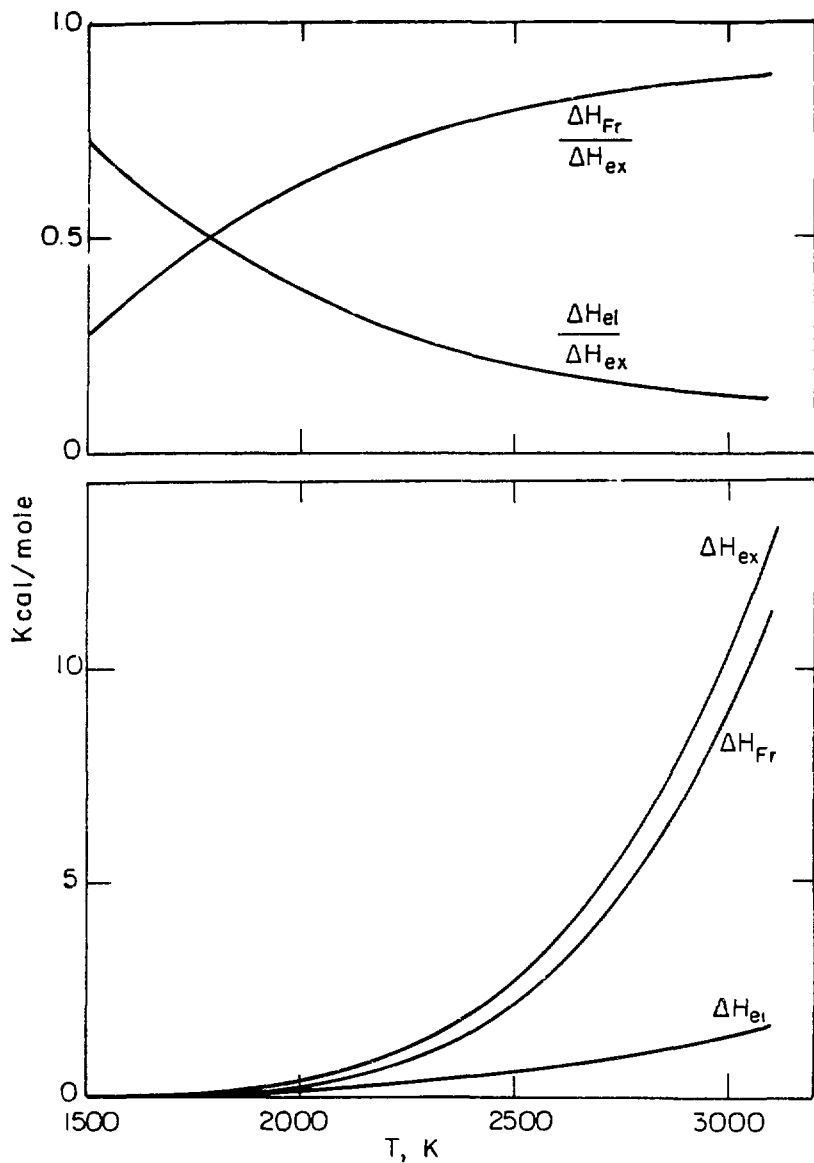
Figure 48. Fitted curve to the enthalpy data of UO_2 between $1000^{\circ}K$ and $3000^{\circ}K$. Lattice vibrational contribution and excess enthalpy are also plotted.

XBL 8011-6350

XBL 801:-6349

Figure 49. Absolute and fractional contributions of Frenkel
disorder and electronic excitation to the excess
enthalpy.

6. CONCLUSIONS

1. Much faster oxygen diffusion in UO_{2-x} than in UO_2 was observed, which proves that the primary defect in UO_{2-x} is the anion vacancy.

2. The measured migration activation energy of the anion vacancy, 11.7 kcal/mole, is lower than the migration energy of interstitials. However, it is not as low as predicted by theoretical calculation [16]. The activation energy and the pre-exponential factor of the oxygen diffusion coefficient are in good agreement with those of other materials of fluorite structure, e.g., CeO_{2-x}, PuO_{2-x}. This confirms the similar oxygen migration mechanisms in these matertials.

3. In stoichiometric UO_2 and near-stoichiometric $UO_{2\pm x}$, both vacancies and interstitials contribute significantly to oxygen diffusion. At 1400°C, contributions of the two species are approximately equal in stoichiometric UO_2. When $T > 1400$°C, the interstitial contribution is higher; when $T < 1400$°C, the vacancy contribution is higher.

4. The Frenkel energy and entropy deduced from measured diffusivities in UO_{2-x}, UO_2 and UO_{2+x} are $\Delta H_F = 85.6$ kcal/mole and $\Delta S_F = 18.2$ e.u. These values yield lower anion Frenkel defect concentration than predicted by Szwarc's model [40]. This deviation is consistent with the theory that not all of the excess enthalpy of UO_2 can be attributed solely to the Frenkel disorder. Use of the ΔH_F and ΔS_F values determined in this study shows that at 3000°K electronic excitation can account for 13 percent of the excess enthalpy.

5. McInnes' [46] two-band model for electronic excitation is modified
   to quantify the electronic enthalpy. Data fitting yields a band
   gap of 2.0 ev, which is in good agreement with the reported
   values [52,53], and effective mass of conduction band electrons of
   7.6 m_e.

ACKNOWLEDGEMENTS

121

REFERENCES

1. J. F. Marin and P. Contamin, J. Nucl. Mater., 30 (1969) 16.

2. A. B. Auskern and J. Belle, J. Nucl. Mater., 3 (1961) 267.

3. P. Contamin, J. J. Backmann, and J. F. Marin, J. Nucl. Mater., 42 (1972) 54.

4. J. Belle, J. Nucl. Mater., 30 (1969) 3.

5. G. E. Murch, Phil. Mag., 32 (1975) 1129.

6. G. E. Murch, D. H. Bradhurst, and H. J. de Bruin, Phil. Mag., 32 (1975) 1141.

7. L. E. Roberts, V. J. Wheeler, and A. Perrin, 1969, unpublished work cited by J. Belle, J. Nucl. Mater., 30 (1969) 3.

8. W. Breitung, J. Nucl. Mater., 74 (1978) 10.

9. G. E. Murch and R. J. Thorn, J. Nucl. Mater., 71 (1978) 219.

10. R. J. Thorn and G. H. Winslow, "Thermodynamics of Nuclear Materials, IAEA, Vienna (1965).

11. P. Contamin, 1971, Doctoral Dissertation, University of Grenoble, CEA-R-4223.

12. J. M. Floyd, Ind. J. of Tech., 11 (1973) 589.

13. B.C.H. Steele and J. M. Floyd, Proc. Brit. Ceram. Soc. 19 (1971) 55.

14. P. Chereau and J. F. Wadier, J. Nucl. Mater., 46 (1973) 1.

15. A. S. Bayoglu and R. Lorenzelli, J. Nucl. Mater., 82 (1979) 403.

16. C.R.A. Catlow and A. B. Lidiard, "Thermodynamics of Nuclear Materials," IAEA, Vienna (1974), Vol. 3, p27.

17. A. E. Martin and R. K. Edwards, J. Phys. Chem., 69 (1965) 1788.

18. R. K. Edwards and A. E. Martin, "Thermodynamics of Nuclear Materials," IAEA, Vienna (1965) vol 2, p423.

19. P. Guinet, H. Vaugoyeau and P. L. Blum, CEA-Report-3060, (1966).

20. S. P. Garg and R. J. Ackermann, J. Nucl. Mater., 88 (1980) 309

21. H. S. Carslaw and J. C. Jaeger, "Conduction of Heat in Solids," 2nd Ed., Oxford, Claredon Press (1959).

22. O. Kubaschewski, E. L. Evans, and C. B. Alcock, "Metallurgical Thermodiomistry," 4th Eds., Pergamon Press, Oxford (1967).

23. N. A. Javed, J. Nucl. Mater., 43 (1972) 219.

24. K. Hagemark and M. Broli, J. Inorg. Nucl. Chem., 23 (1966) 2837.

25. V. J. Wheeler and J. G. Jones, J. Nucl. Mater., 42 (1972) 117.

26. M. Tetenbaum and P. D. Hunt, J. Chem. Phys., 49 (1968) 4739.

27. T. L. Markin, V. J. Wheeler, and R. J. Bones, J. Inorg. Nucl. Chem., 30 (1968) 807.

28. P. E. Blackburn, J. Nucl. Mater., 46 (1973) 244.

29. A. N. Nesmeianov, "Vapor Pressures of the Chemical Elements," R. Gray, Ed., Elsevier Publishing Co. (1963).

30. R. C. Reid and T. K. Sherwood, "The Properties of Gases and Liquids," 2nd Ed. pp 523-525, McGraw-Hill Book Co., N.Y. (1960).

31. M. Tetenbaum and P. D. Hunt, J. Nucl. Mater., 34 (1970) 86.

32. J. L. Drummond and V. M. Sinclair, 6th Conference on Analytical Chemistry, Gatlinburg, USAEC Report TID-7655, pp 217-239 (1962).

33. T. L. Markin and R. J. Bones, AERE-R4178 (1964).

34. I. G. Jones, AERE-R-6962 (1973).

35. C. E. McNeilly and T. D. Chikalla, J. Nucl. Mater., 39 (1971) 77.

36. C. F. Robinson, Chapter 16, "Microprobe Analysis," ed. C. A. Anderson, Wiley-Interscience (1973).

37. L. R. Valencourt, C. E. Johnson, and D. V. Steidl, J. Nucl. Mater., 58 (1975) 293.

38. R. E. Fryxell, D. E. Joyce, and R. Szwarc, J. Nucl. Mater., 25 (1968) 97.

39. P. Kofstad, "Nonstoichiometry, Diffusion and Electrical Conductivity in Binary Metal-oxides," Wiley-Interscience (1972).

40. R. Szwarc, J. Phys. Chem. Solids, 30 (1969) 705.

41. A. E. Ogard and J. A. Leary, "Thermodynamics of Nuclear Materials," IAEA, Vienna (1967).

42. R. A. Hein, L. H. Sjodhl, and R. Szwarc, J. Nucl. Mater., 25 (1968) 99.

43. L. Leibowitz, L. W. Mishler, and M. G. Chasanov, J. Nucl. Mater., 29 (1969) 356.

44. J. F. Kerrisk and D. G. Clifton, Nucl. Technol., 16 (1972) 531.

45. C.R.A. Catlow, Proc. Roy. Soc. (London) A353 (1977) 533.

46. D. A. MacInnes, J. Nucl. Mater., 78 (1978) 225.

47. R. J. Thorn, G. H. Winslow, and J. S. Ziomek, J. Nucl. Mater., 87 (1979) 416.

48. D. A. MacInnes and C.R.A. Catlow, J. Nucl. Mater., 89 (1980) 354.

49. M. O'Keefe, "Chemistry of Extended Defects in Non-Metallic Solids," L. Eyring and M. O'Keefe Ed., North-Holland (1970).

50. D. R. Frederickson and M. G. Chasanov, J. Chem. Thermodynamics, 2 (1970) 623.

51. R. A. Hein, P. N. Flagella, and J. B. Conway, J. Am. Ceram. Soc., 51 (1968) 291.

52. J. L. Bates, C. A. Hinman, and T. Kawada, J. Am. Ceram. Soc., 50 (1967) 652.

53. J. Schoenes, J. Appl. Phys., 49 (1978) 1463.

54. P. E. Blackburn, J. Nucl. Mater., 46 (1973) 244.